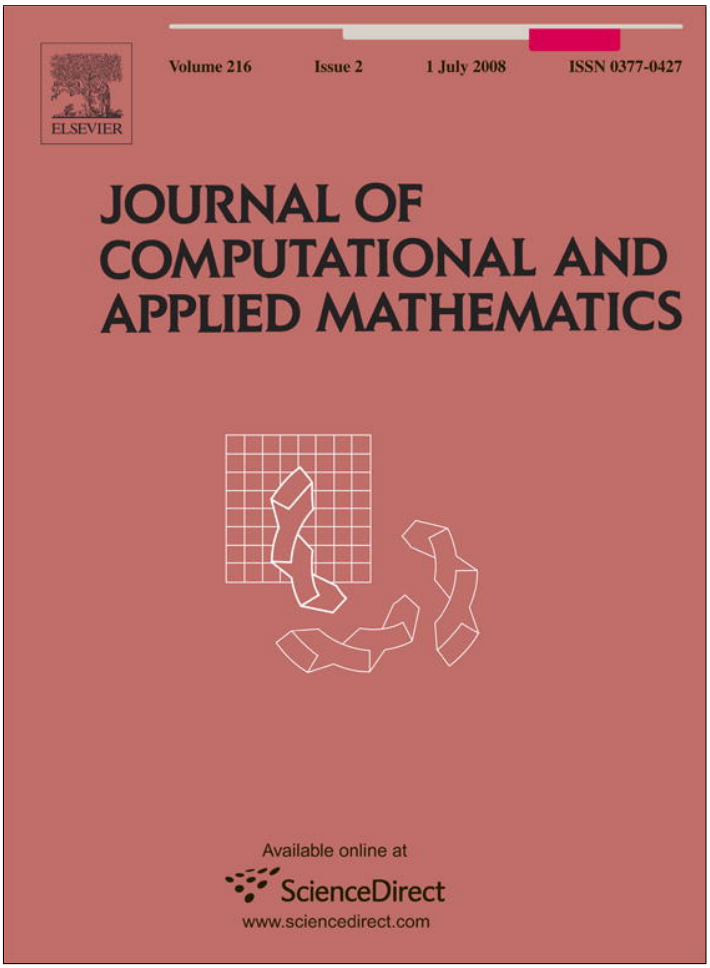

Available online at www.sciencedirect.com
ScienceDirect
Journal of Computational and Applied Mathematics 216 (2008) 388–412
JOURNAL OF COMPUTATIONAL AND APPLIED MATHEMATICS
www.elsevier.com/locate/cam

A geometrical method for the approximation of invariant tori☆

Bryan Rasmussen[a,*], Luca Dieci[b]

[a] *Los Alamos National Laboratory, MS T080 Los Alamos, NM 87545, USA*
[b] *School of Mathematics, Georgia Institute of Technology, Atlanta, GA 30332-0160, USA*

Received 22 August 2006; received in revised form 25 January 2007

Abstract

We consider a numerical method based on the so-called "orthogonality condition" for the approximation and continuation of invariant tori under flows. The basic method was originally introduced by Moore [Computation and parameterization of invariant curves and tori, SIAM J. Numer. Anal. 15 (1991) 245–263], but that work contained no stability or consistency results. We show that the method is unconditionally stable and consistent in the special case of a periodic orbit. However, we also show that the method is unstable for two-dimensional tori in three-dimensional space when the discretization includes even numbers of points in both angular coordinates, and we point out potential difficulties when approximating invariant tori possessing additional invariant sub-manifolds (e.g., periodic orbits). We propose some remedies to these difficulties and give numerical results to highlight that the end method performs well for invariant tori of practical interest.

MSC: 37M99; 65P99

Keywords: Numerical analysis; Invariant manifolds; Invariant tori

1. Introduction

The goal of this paper is to analyze a method for the numerical approximation of flow-invariant tori in real spaces. Typically, the practical use of such method is in a continuation context. Consider the autonomous system of ordinary differential equations with a $\mathscr{C}^k$, $k \geqslant 2$, vector field

$$\dot{\mathbf{x}} = \mathbf{\Phi}(\mathbf{x}, \lambda), \quad \mathbf{x} \in \mathbb{R}^n, \quad \lambda \in \mathbb{R}. \tag{1}$$

The goal is to approximate a torus that is invariant under the flow generated by the differential system for a particular value of λ, and then to continue the torus in λ. The role of λ is immaterial in all that follows, except that during continuation there is an initial approximation for the current invariant torus from another torus that is invariant at a previous λ value; for this reason, we will henceforth just write $\mathbf{\Phi}(\mathbf{x})$ for the vector field.

In the last 15 years, there has been considerable interest in approximation of invariant tori of dynamical systems, a topic which continues to attract the attention of several researchers also at the theoretical level, as witnessed by the recent works [4,5] which are relevant for quasi-periodic invariant tori of maps. For numerical techniques,

☆ This work was supported in part under NSF Grant DMS 0139895.
* Corresponding author. Tel.: +1 505 6673148; fax: +1 505 6677665.
E-mail addresses: bryanras@lanl.gov (B. Rasmussen), dieci@math.gatech.edu (L. Dieci).

0377-0427/$ - see front matter © 2007 Elsevier B.V. All rights reserved.
doi:10.1016/j.cam.2007.05.025

see [3,6,7,10,12,13,23,22,24–26,29,30] for methods concerned with approximation of invariant tori in general and [17,28] for techniques specifically concerned with quasi-periodic invariant tori. We refer to the recent work [28] for a well-written and comprehensive review of the existing techniques. Quasi-periodic invariant tori are of course of great interest, especially in the context of Hamiltonian dynamics (e.g., see [18,21]). However, it is well known that invariant tori may persist while quasi-periodic motion does not, so here we are interested in techniques which are not restricted to quasi-periodic tori.

Unfortunately, several of the numerical methods which have been proposed in the above works lack a rigorous stability analysis. Therefore, methods that seem to work well in practice may instead be subject to instabilities as they are applied to more problems. For example, the original discretization proposed in [10] was later realized to be unstable in general, a fact which prompted consideration of a different, provably stable, discretization in [7]. Also the discretization schemes proposed in [12,22,23,13,29,28] lack a complete theoretical justification, i.e., a stability analysis, although the authors' computational sensibility has probably led to trustworthy numerical results. Nevertheless, approximation of invariant tori is a delicate computational task, and it is important to have rigorous stability analyses of the numerical methods. Likewise, conditional stability results, or stability results for realistic model problems, as well as instability results, are all important, because they help us to understand how to use a certain scheme properly. Our chief goal in this work is to rectify at least in part the lack of rigorous analysis, relative to a specific technique, the so-called "orthogonality technique" originally introduced by Moore in [22,23].

Most general numerical methods for approximation of invariant tori essentially require the solution of a PDE either directly [6,7,10,12,13,28,29] or indirectly through the Hadamard graph transform [8,24,30]. In general, direct solution methods for invariant tori require significant *a priori* preparation, namely the appropriate choice and update of a coordinate system in which to represent the sought-after torus. For quasi-periodic tori, in [28] the authors propose a method where the vector of the frequencies is treated as unknown, and updated during continuation as well; although one can try this approach also for general tori, the method is designed for quasi-periodic tori. On the other hand, graph transform techniques remain generally applicable; their primary shortcomings are that they require an integration of the vector field, and the graph transform technique is only linearly convergent. (Osinga uses Newton's method in [24], and this clearly speeds up the iteration, the trade-off being an increase in storage and in the linear algebra expense.) In [22,23], Moore explores a completely different avenue that avoids integration of the vector field. Thanks to clever geometrical insight, he proposes a new condition to characterize the invariant torus; we call it the *orthogonality condition*.

To set the stage, let $T^p = (\mathbb{R}/2\pi)^p$ denote the standard p-torus, and let $q := n - p$. We assume that the invariant torus has a $\mathscr{C}^2$-smooth embedding, $\mathbf{x}^* : T^p \to \mathbb{R}^n$, and also that the derivative of $\mathbf{x}^*$ with respect to $\boldsymbol{\phi}$, $D_{\boldsymbol{\phi}}\mathbf{x}^*(\boldsymbol{\phi}) \in \mathbb{R}^{n\times p}$, is full-rank at all $\boldsymbol{\phi}$. As a consequence, there is a $\mathscr{C}^1$ moving system of normal vectors, stored as columns of a matrix, $Q : T^p \to \mathbb{R}^{n\times q}$. The orthogonality condition simply states that $\mathbf{x}^*$ is invariant under the flow of (1) for a particular λ if and only if it satisfies

$$Q(\boldsymbol{\phi})^{\mathrm{T}}\boldsymbol{\Phi}(\mathbf{x}^*(\boldsymbol{\phi})) = \mathbf{0}. \tag{2}$$

To develop a method based on the orthogonality condition, one requires that (2) be satisfied relative to some points of a grid. The outstanding difficulty is how to define the normal vectors in Q in such a way that computing Q is inexpensive and Q perturbs smoothly with small changes in the torus. In [22], Moore proposes a numerical method based on a discretization of (2). The method proposed in [22] is a box scheme (second-order accurate discretization), but no stability analysis for the method is given in [22]. Our goal in this paper is to analyze the basic numerical technique for (2), and a main result of ours will be to show that, in general, the technique is unstable. Although limited to a particular scheme for the orthogonality condition, we believe that our analysis should prove useful to infer potential instabilities also for other existing discretization methods (especially second and higher order of consistency) for invariant tori; see also Remark 2.1 later on.

Remark 1.1. The algorithms developed by Moore in [22] are somewhat different from the basic algorithm that we are able to analyze here. The main difference is that Moore implements a sophisticated, quasi-conformal grid redistribution strategy for 2-tori, while we rely on simpler strategies as they become necessary. There are also two other minor differences: (i) in [22], the computation of the instantaneous normal directions is done differently in general than how we will do it, although for 2-tori embedded in $\mathbb{R}^3$ it is the same as we do; (ii) in [22], the author uses a quasi-Newton update instead of a full Newton iteration, as we do. We believe that these two algorithmic differences are not strong

enough to impact our conclusions. Instead, it may be interesting, but apparently quite hard, to understand to what extent the mesh redistribution prevents or hides the instabilities of the basic scheme.

A plan of this paper is as follows. In Section 2 we clarify the equivalence between the orthogonality condition and the PDE formulation. In Section 3 we consider computation of Q and the resulting discretization scheme. In Section 4 we prove that the scheme is stable for periodic orbits (1-tori), whereas in Section 5 we show that, in certain circumstances, the method is unconditionally unstable even if one has a canonical choice for the normal vectors (and in such cases, our technique is essentially that of [22]). Specifically, the method can encounter difficulty if the discretization includes too many even numbers of points in the different angular directions, or if the invariant torus admits invariant sub-manifolds. Practical remedies are proposed in the context of Section 6, where we present results of numerical experiments on problems from the literature. Conclusions are in Section 7.

Notation

This paper uses a convention for labeling variables:

(i) Asterisks ($\mathbf{x}^*$) denote actual invariant tori and smooth approximations.
(ii) Overbars ($\overline{\mathbf{x}}$) denote initial guesses and reference states.
(iii) Karats ($\widehat{\mathbf{x}}$) denote updates and modifications of initial guesses.
(iv) Tildes ($\widetilde{Q}$) denote averages taken at the centers of boxes in the discretization scheme.

2. Equivalence of orthogonality and PDE conditions

At a general level, the approximation process comprises two steps: (1) choose a suitable condition that the sought-after invariant torus satisfies, and (2) discretize that condition to obtain an approximation of the torus. Two such conditions are the PDE and orthogonality conditions, both of which rely on a local representation of the torus with respect to some initial guess (often, a torus computed at a previous parameter value in the continuation process).

Definition 1. Let T^p be a p-torus with coordinate $\boldsymbol{\phi}$. Let $\overline{\mathbf{x}} : T^p \to \mathbb{R}^n$ be a $\mathscr{C}^2$-smooth embedding, and let $\overline{Q} : T^p \to \mathbb{R}^{n\times(n-p)}$ be a $\mathscr{C}^1$-smooth function such that at each $\boldsymbol{\phi} \in T^p$, the columns of $\overline{Q}(\boldsymbol{\phi})$ form an orthonormal basis of the normal space to the graph of $\overline{\mathbf{x}}$ at $\boldsymbol{\phi}$. Then the pair $[\overline{\mathbf{x}}, \overline{Q}]$ is called a *reference torus*.

For convenience, the term "reference torus" may also apply to the embedding $\overline{\mathbf{x}}$ or its graph rather than the pair $[\overline{\mathbf{x}}, \overline{Q}]$. In a sufficiently small tubular neighborhood around a reference torus, every point has a unique representation in a local $(\boldsymbol{\phi}, \boldsymbol{\rho})$ coordinate system: $\mathbf{x}(\boldsymbol{\phi}, \boldsymbol{\rho}) = \overline{\mathbf{x}}(\boldsymbol{\phi}) + \overline{Q}(\boldsymbol{\phi})\boldsymbol{\rho}$.

We assume that the actual invariant torus, $\mathbf{x}^*$, is sufficiently close to the reference torus in the sense that there exists a unique representation in terms of a $\mathscr{C}^1$ function, $\mathbf{r} : T^p \to \mathbb{R}^q$,

$$\mathbf{x}^*(\boldsymbol{\phi}) = \overline{\mathbf{x}}(\boldsymbol{\phi}) + \overline{Q}(\boldsymbol{\phi})\mathbf{r}(\boldsymbol{\phi}). \tag{3}$$

The PDE condition relies explicitly on the local representation (3) of the invariant torus. In principle, in a tubular neighborhood of the reference torus, the vector field splits into tangential-normal coordinates,

$$\boldsymbol{\Phi} = (\dot{\boldsymbol{\phi}}, \dot{\boldsymbol{\rho}}), \tag{4}$$

though $\dot{\boldsymbol{\phi}}$ and $\dot{\boldsymbol{\rho}}$ may be difficult to derive in a closed form. With $\mathbf{r}(\boldsymbol{\phi})$ defining the actual invariant torus as in (3), then a necessary and sufficient invariance condition for $\mathbf{x}^*$ is that the time derivative of $\mathbf{r}$ be the normal component of the vector field [10]. That is, $\mathbf{r}$ has to satisfy the *PDE condition*

$$[D_{\boldsymbol{\phi}}\mathbf{r}(\boldsymbol{\phi})]\dot{\boldsymbol{\phi}}(\boldsymbol{\phi}, \mathbf{r}(\boldsymbol{\phi})) = \dot{\boldsymbol{\rho}}(\boldsymbol{\phi}, \mathbf{r}(\boldsymbol{\phi})). \tag{5}$$

The solution of this first-order PDE, subject to periodic boundary conditions, characterizes the invariant torus. As mentioned in the "Introduction", directly solving this PDE (e.g., as done in [6,10,12,13,29]) can be tricky. Regardless,

transforming the vector field into local coordinates to obtain the PDE in the first place is not always straightforward. Thus, techniques based on the PDE condition have been devised so not solve (5) directly but rather use the Hadamard graph transform, which can be thought of as a solution technique using the method of characteristics [8].

The orthogonality condition, in contrast, does not require the solution of a PDE, but instead relies on an instantaneous description of normal spaces. We consider tori in the form of (3) and equip them with a smoothly varying system of orthonormal vectors, $Q(\boldsymbol{\phi})$, which are orthogonal to the tangent vectors of the graph of $\mathbf{x}^*$ at $\boldsymbol{\phi}$. The formal requirement on $Q(\boldsymbol{\phi})$ is as follows.

Q must satisfy three properties:

(i) The mapping $Q: (\boldsymbol{\phi}, D_{\boldsymbol{\phi}}\mathbf{x}^*(\boldsymbol{\phi})) \in T^p \times \mathbb{R}^{n\times p} \to Q(\boldsymbol{\phi}, D_{\boldsymbol{\phi}}\mathbf{x}^*(\boldsymbol{\phi})) \in \mathbb{R}^{n\times q}$ is at least $\mathscr{C}^1$.
(ii) Q has orthonormal columns.
(iii) The columns of Q lie in the normal space, so $Q(\boldsymbol{\phi}, D_{\boldsymbol{\phi}}\mathbf{x}^*(\boldsymbol{\phi}))^{\mathrm{T}} D_{\boldsymbol{\phi}}\mathbf{x}^*(\boldsymbol{\phi}) = \mathbf{0}$.

For fixed $\mathbf{x}^*$, we refer to Q as a function from T^p only, so we may write $Q(\boldsymbol{\phi}) = Q(\boldsymbol{\phi}, D_{\boldsymbol{\phi}}\mathbf{x}^*(\boldsymbol{\phi}))$. Given such a rule Q for calculating normal spaces, one can characterize invariance for $\mathbf{x}^*$ by stating that the vector field has no component in the normal directions at any point on the graph of $\mathbf{x}^*$. This gives the *orthogonality condition* in (2).

At a high level, equivalence between the PDE condition (5) and the orthogonality condition (2) is clear, since both characterize an invariant torus. Nevertheless, it is insightful to highlight the algebraic equivalence between these two conditions.

Proposition 2. *Let* $[\overline{\mathbf{x}}, \overline{Q}]$ *be a reference torus, and let* $\mathbf{x}^*$ *be as in* (3). *Then* $\mathbf{x}^*$ *satisfies* (5) *if and only if it satisfies* (2). *Moreover*, $\mathbf{x}^*$ *satisfies these two conditions if and only if it satisfies*

$$[D_{\boldsymbol{\phi}}\mathbf{x}^*(\boldsymbol{\phi})]\dot{\boldsymbol{\phi}} = \boldsymbol{\Phi}(\mathbf{x}^*(\boldsymbol{\phi})). \tag{6}$$

Proof. The total derivative of $\mathbf{x}^*$ with respect to time is

$$[D_{\boldsymbol{\phi}}\mathbf{x}^*(\boldsymbol{\phi})]\dot{\boldsymbol{\phi}} = ([D_{\boldsymbol{\phi}}\overline{\mathbf{x}}(\boldsymbol{\phi})] + [D_{\boldsymbol{\phi}}\overline{Q}(\boldsymbol{\phi})\boldsymbol{\rho}]_{\boldsymbol{\rho}=\mathbf{r}(\boldsymbol{\phi})} + \overline{Q}(\boldsymbol{\phi})[D_{\boldsymbol{\phi}}\mathbf{r}(\boldsymbol{\phi})])\dot{\boldsymbol{\phi}}, \tag{7}$$

and the vector field evaluated at a point $\mathbf{x}^*(\boldsymbol{\phi})$ is

$$\boldsymbol{\Phi}(\mathbf{x}^*(\boldsymbol{\phi})) = [D_{\boldsymbol{\phi}}\overline{\mathbf{x}}(\boldsymbol{\phi})]\dot{\boldsymbol{\phi}} + [D_{\boldsymbol{\phi}}\overline{Q}(\boldsymbol{\phi})\boldsymbol{\rho}]_{\boldsymbol{\rho}=\mathbf{r}(\boldsymbol{\phi})}\dot{\boldsymbol{\phi}} + \overline{Q}(\boldsymbol{\phi})\dot{\boldsymbol{\rho}}. \tag{8}$$

The above two equations combine to form

$$[D_{\boldsymbol{\phi}}\mathbf{x}^*(\boldsymbol{\phi})]\dot{\boldsymbol{\phi}} = \boldsymbol{\Phi}(\mathbf{x}^*(\boldsymbol{\phi})) + \overline{Q}(\boldsymbol{\phi})([D_{\boldsymbol{\phi}}\mathbf{r}(\boldsymbol{\phi})]\dot{\boldsymbol{\phi}} - \dot{\boldsymbol{\rho}}). \tag{9}$$

We multiply both sides by $Q(\boldsymbol{\phi})^{\mathrm{T}}$ and note that $Q(\boldsymbol{\phi})^{\mathrm{T}} D_{\boldsymbol{\phi}}\mathbf{x}^*(\boldsymbol{\phi}) = \mathbf{0}$ to obtain

$$Q(\boldsymbol{\phi})^{\mathrm{T}}\boldsymbol{\Phi}(\mathbf{x}^*(\boldsymbol{\phi})) + Q(\boldsymbol{\phi})^{\mathrm{T}}\overline{Q}(\boldsymbol{\phi})([D_{\boldsymbol{\phi}}\mathbf{r}(\boldsymbol{\phi})]\dot{\boldsymbol{\phi}} - \dot{\boldsymbol{\rho}}) = \mathbf{0}. \tag{10}$$

Therefore, if $\mathbf{x}^*$ satisfies (5), then it satisfies (2). Conversely, for $\mathbf{x}^*$ parameterizable in the form of (3), the product $Q(\boldsymbol{\phi})^{\mathrm{T}}\overline{Q}(\boldsymbol{\phi})$ is invertible, so if $\mathbf{x}^*$ satisfies (2), it must also satisfy (5).

To prove equivalence with (6), we note that if $\mathbf{x}^*$ satisfies the PDE condition, then (9) implies that it satisfies (6). The converse follows because multiplying both sides of (6) by $Q(\boldsymbol{\phi})^{\mathrm{T}}$ and $\overline{Q}(\boldsymbol{\phi})^{\mathrm{T}}$ results in the orthogonality and PDE conditions, respectively. □

The most important implication of the above proposition is that the PDE and orthogonality conditions both descend from the same equation, (6). The two conditions simply represent different ways of reducing the dimensionality of (6) and thus making the problem well-posed. We should note, too, that there is nothing special about tori in the above discussion apart from the parameterization in $\boldsymbol{\phi}$. All the results so far have analogs for any closed, compact, orientable manifold with a proper parameterization, invariant under the flow of (1).

Remark 2.1. There is one final consequence of the equivalence between the PDE condition and other explicit invariance conditions: Any discretization of an invariance condition generates an implied discretization of the PDE. While this

implied discretization may be quite complicated, we can infer instability in certain cases by considering the discretization of the PDE. Specifically, it must be true that *any* discretization of *any* invariance condition that is equivalent to the PDE will be subject to instability if the implied discretization of the PDE is unstable. We believe that this explains the observation in Section 6 that when the grid "lines up" with a periodic orbit the scheme becomes unstable. In practice, one may be able to avoid instability by choosing a grid (or a discretization) wisely, just as it is necessary to do when solving hyperbolic PDE by finite-differences.

3. Discretization of orthogonality condition

The types of discretizations investigated here are called *box schemes*. These schemes represent the torus as an ordered set of p-dimensional boxes and approximate the normal directions at the center of each box using information from the 2^p vertices. A more precise discussion requires some standard terminology. Recall the term *reference torus* in Definition 1.

A *grid* on a reference torus is a lexicographically ordered sequence,

$$[\overline{\mathbf{x}}_{i_1,i_2,\ldots,i_p}, \overline{Q}_{i_1,i_2,\ldots,i_p}],$$

where $i_k = 1, 2, \ldots, N_k$, with toroidal periodicity. An *update* of a grid is a sequence of points of the form

$$\widehat{\mathbf{x}}_{i_1,i_2,\ldots,i_p} = \overline{\mathbf{x}}_{i_1,i_2,\ldots,i_p} + \overline{Q}_{i_1,i_2,\ldots,i_p}\mathbf{r}_{i_1,i_2,\ldots,i_p}. \tag{11}$$

Occasionally, the term "update" will refer to the list of normal distances, $\{\mathbf{r}_{i_1,i_2,\ldots,i_p}\}$, rather than the points themselves.

The existence of a grid with a toroidal ordering implies the existence of boxes on the reference torus or on an update. For example, for any given point on an update, $\widehat{\mathbf{x}}_{i_1,i_2,\ldots,i_p}$, a *box* is a set of 2^p points, $\{\widehat{\mathbf{x}}_{i'_1,i'_2,\ldots,i'_p}\}$, such that $i'_k = i_k$ or $i'_k = i_k + 1$ for each k. The points in a box are called *vertices*.

Each box on an update gives rise to a canonical set of p tangent vectors, $\widehat{\mathbf{x}}_-^{(1)}, \widehat{\mathbf{x}}_-^{(2)}, \ldots, \widehat{\mathbf{x}}_-^{(p)}$. For example, in a limit cycle, the tangent vector is

$$\widehat{\mathbf{x}}_-^{(1)} = \widehat{\mathbf{x}}_{i+1} - \widehat{\mathbf{x}}_i. \tag{12}$$

In a 2-torus, the tangent vectors are

$$\widehat{\mathbf{x}}_-^{(1)} = (\widehat{\mathbf{x}}_{i+1,j} - \widehat{\mathbf{x}}_{i,j}) + (\widehat{\mathbf{x}}_{i+1,j+1} - \widehat{\mathbf{x}}_{i,j+1}),$$

and

$$\widehat{\mathbf{x}}_-^{(2)} = (\widehat{\mathbf{x}}_{i,j+1} - \widehat{\mathbf{x}}_{i,j}) + (\widehat{\mathbf{x}}_{i+1,j+1} - \widehat{\mathbf{x}}_{i+1,j}). \tag{13}$$

In general, for a p-torus there are p tangent vectors in each box that are the sums of 2^{p-1} differences. These vectors represent tangent directions at the center of the box. (Note the suppression of the referencing subscript. No calculations for the remainder of this paper will mix tangent vectors from different boxes, so it is not necessary to denote box coordinates in the $\widehat{\mathbf{x}}_-^{(i)}$ notation.)

In Section 5, we use a simplified version of (13). Since the ultimate goal is to compute normal directions, several definitions of tangent vectors will suffice, so long as they span the same space. The following formulation is equivalent to (13) for a 2-torus embedded in $\mathbb{R}^3$:

$$\widehat{\mathbf{x}}_-^{(1)} = (\widehat{\mathbf{x}}_{i+1,j+1} - \widehat{\mathbf{x}}_{i,j}),$$

and

$$\widehat{\mathbf{x}}_-^{(2)} = (\widehat{\mathbf{x}}_{i+1,j} - \widehat{\mathbf{x}}_{i,j+1}). \tag{14}$$

Some grids are better than others for numerical purposes. The following criteria restrict the possible grids by using a scalar representation of acceptability.

Definition 3. A *δ-grid* on a reference torus is a grid that satisfies three properties:

(i) The shortest arc length distance along the surface of the torus between any two points in the same box is less than δ.
(ii) The minimum angle between any two distinct tangent vectors $\overline{\mathbf{x}}_-^{(i)}$ and $\overline{\mathbf{x}}_-^{(j)}$ in the same box is large enough that

$$|(\overline{\mathbf{x}}_-^{(i)})^{\mathrm{T}}\overline{\mathbf{x}}_-^{(j)}| < \delta\|\overline{\mathbf{x}}_-^{(i)}\|\,\|\overline{\mathbf{x}}_-^{(j)}\|. \tag{15}$$

(iii) For all tangent vectors, $\overline{\mathbf{x}}_-^{(i)}$ and $\overline{\mathbf{x}}_-^{(j)}$, in the same box,

$$\|\overline{\mathbf{x}}_-^{(i)}\|/\|\overline{\mathbf{x}}_-^{(j)}\| > 1 - \delta. \tag{16}$$

In other words, making δ small ensures that a δ-grid is not overly coarse, skewed, or elongated in any particular box. Depending on the size of the torus, the δ required for the first property in the definition may be of a different order of magnitude than the δ required for the other two properties, so a more flexible definition would include a fixed constant times δ in the first property. We omit this extra constant for simplicity.

Stability/instability arguments will require closeness of solutions to the reference torus in a $\mathscr{C}^1$ sense (not just a $\mathscr{C}^0$ sense). Discrete solutions are collections of points, not functions, so it is necessary to extend the notion of $\mathscr{C}^1$-closeness to numerical representations of tori.

Definition 4. An *α-update* of a grid is an update that satisfies

(i) $\|\mathbf{r}_{i_1,i_2,\ldots,i_p}\| < \alpha$ at all points of the grid, and
(ii) If $\overline{\mathbf{x}}_\mathbf{a}$ and $\overline{\mathbf{x}}_\mathbf{b}$ are two distinct points in the same box then

$$1 - \alpha < \frac{\|\widehat{\mathbf{x}}_\mathbf{a} - \widehat{\mathbf{x}}_\mathbf{b}\|}{\|\overline{\mathbf{x}}_\mathbf{a} - \overline{\mathbf{x}}_\mathbf{b}\|} < 1 + \alpha, \tag{17}$$

and

$$(\widehat{\mathbf{x}}_\mathbf{a} - \widehat{\mathbf{x}}_\mathbf{b})^{\mathrm{T}}(\overline{\mathbf{x}}_\mathbf{a} - \overline{\mathbf{x}}_\mathbf{b}) > (1 - \alpha)\|\widehat{\mathbf{x}}_\mathbf{a} - \widehat{\mathbf{x}}_\mathbf{b}\|\,\|\overline{\mathbf{x}}_\mathbf{a} - \overline{\mathbf{x}}_\mathbf{b}\|. \tag{18}$$

The second two inequalities in Definition 4 essentially constrain the difference between derivatives on the reference torus and the update. It is now possible to define box schemes formally.

Definition 5. A reference torus is equipped with a *box scheme* if for every δ-grid with δ sufficiently small, there exists α such that for every α-update and every index $i_1, i_2, \ldots, i_p$, there is a rule for generating a matrix, $\widetilde{Q}_{i_1,i_2,\ldots,i_p} \in \mathbb{R}^{n\times q}$, whose orthonormal columns are orthogonal to the tangent vectors $\widehat{\mathbf{x}}_-^{(1)}, \widehat{\mathbf{x}}_-^{(2)}, \ldots, \widehat{\mathbf{x}}_-^{(p)}$. Additionally, $\widetilde{Q}_{i_1,i_2,\ldots,i_p}$ must perturb smoothly with the update, and for any two members of the same box, $\widehat{\mathbf{x}}_{i_1,i_2,\ldots,i_p}$ and $\widehat{\mathbf{x}}_{i'_1,i'_2,\ldots,i'_p}$, $\|\widetilde{Q}_{i_1,i_2,\ldots,i_p} - \widetilde{Q}_{i'_1,i'_2,\ldots,i'_p}\|$must be of order $\|\widehat{\mathbf{x}}_{i_1,i_2,\ldots,i_p} - \widehat{\mathbf{x}}_{i'_1,i'_2,\ldots,i'_p}\|$.

Given such a scheme, the discrete version of (2) is

$$\widetilde{Q}^{\mathrm{T}}_{i_1,i_2,\ldots,i_p}\mathbf{\Phi}(\widetilde{\mathbf{x}}_{i_1,i_2,\ldots,i_p}) = \mathbf{0}, \tag{19}$$

where $\widetilde{\mathbf{x}}_{i_1,i_2,\ldots,i_p}$ denotes the average of all points in the box corresponding to the point $i_1, i_2, \ldots, i_p$ on the update. We will use a full Newton iteration to find the update $\{\mathbf{r}_{i_1,i_2,\ldots,i_p}\}$ that solves (19), but first we propose a general box scheme for computing the normal vectors $\widetilde{Q}_{i_1,i_2,\ldots,i_p}$.

Two special cases admit canonical box schemes up to sign. For these two cases, our discretization choice is the same choice of Moore [22].

(i) First, if the reference torus is actually a cycle in the plane, then at the center of the box i,

$$\widetilde{Q}_i = \pm\begin{pmatrix} 0 & 1 \\ -1 & 0 \end{pmatrix}(\widehat{\mathbf{x}}_{i+1} - \widehat{\mathbf{x}}_i)/\|\widehat{\mathbf{x}}_{i+1} - \widehat{\mathbf{x}}_i\|. \tag{20}$$

(ii) Second, if the reference torus is a 2-torus embedded in $\mathbb{R}^3$, then the canonical normal vector is

$$\widetilde{Q}_{i,j} = \pm\widehat{\mathbf{x}}_-^{(1)} \times \widehat{\mathbf{x}}_-^{(2)} / \|\widehat{\mathbf{x}}_-^{(1)} \times \widehat{\mathbf{x}}_-^{(2)}\|, \tag{21}$$

where $\widehat{\mathbf{x}}_-^{(1)}$ and $\widehat{\mathbf{x}}_-^{(2)}$ are as in (13) or, equivalently, (14).

When $\widetilde{Q}$ is a single vector, we write it as $\widetilde{\mathbf{n}}$ below. Also, we suppress the subscript under $\widetilde{Q}$ or $\widetilde{\mathbf{n}}$ when we perform operations on a single box.

The box scheme in (i) above generally leads to a stable method as long as the cycle does not contain any fixed points. However, we show in the next section that for the box scheme in (ii) the use of even numbers of points in both angular directions of the grid will cause the method to be unconditionally unstable. We say that a method is "stable" if, for an isolated invariant torus, a sufficiently close reference torus, and a sufficiently regular grid, the discrete equations in (19) have a unique, isolated solution.

Before exploring stability properties, we first discretize the orthogonality condition in the general case of a p torus in $\mathbb{R}^n$, that is we discuss how we find $\widetilde{Q}_{i_1,i_2,\ldots,i_p}$. The way we do this differs from the work [22], where a global solution to an orthogonal Procrustes problem is used.

Given a reference torus, δ-grid, and α-update with δ and α sufficiently small, our goal is to calculate the orthogonal matrices $\widetilde{Q}_{i_1,i_2,\ldots,i_p}$—that is, the normal vectors at the center of each box—using only information from the box itself. One way to obtain normal directions is to orthonormalize the tangent vectors by a complete QR decomposition using Householder reflections [14]:

$$(\widehat{\mathbf{x}}_-^{(1)} \;\; \widehat{\mathbf{x}}_-^{(2)} \;\; \cdots \;\; \widehat{\mathbf{x}}_-^{(p)}) = QR = (T \;\; \widetilde{Q})R, \tag{22}$$

where $Q \in \mathbb{R}^{n\times n}$ is orthogonal and $R \in \mathbb{R}^{n\times p}$ is upper triangular with positive diagonal entries. The first p columns of Q (i.e., T) are the orthonormalized set of tangent vectors, and the next q columns (i.e., $\widetilde{Q}$) span the normal complement. Unfortunately, this simple approach leads to discontinuities in $\widetilde{Q}$, because small perturbations in the tangent vectors can change the ordering of some of the last q columns of Q.

We correct this approach by using *a priori* information about the direction of the normal vectors. In particular, we stabilize the QR decomposition by seeding it with approximate normal vectors from the reference torus. We notice that this approach was already considered in [27, p. 172].

By assumption, the matrices $\overline{Q}_{i_1,i_2,\ldots,i_p}$ store q vectors that are normal to the reference torus at grid points. If we let $(\overline{Q}_{\text{ave}})_{i_1,i_2,\ldots,i_p}$ be the average of the $\overline{Q}$'s along the vertices of the box corresponding to the grid point $(i_1, i_2, \ldots, i_p)$, then for a given α-update with α sufficiently small, the columns of $(\overline{Q}_{\text{ave}})_{i_1,i_2,\ldots,i_p}$ will not lie in the span of $\widehat{\mathbf{x}}_-^{(1)}, \widehat{\mathbf{x}}_-^{(2)}, \ldots, \widehat{\mathbf{x}}_-^{(p)}$. We therefore seed the decomposition with $(\overline{Q}_{\text{ave}})_{i_1,i_2,\ldots,i_p}$, and use the corrected version of (22)

$$(\widehat{\mathbf{x}}_-^{(1)} \;\; \widehat{\mathbf{x}}_-^{(2)} \;\; \cdots \;\; \widehat{\mathbf{x}}_-^{(p)} \;\; (\overline{Q}_{\text{ave}})_{i_1,i_2,\ldots,i_p}) = (T \;\; \widetilde{Q})R, \tag{23}$$

where now $R \in \mathbb{R}^{n\times n}$ is upper triangular with positive diagonal entries. This gives a smoothly varying set of normal vectors at the center of each box.

To reiterate, the algorithm for approximating an invariant torus requires two main items:

(i) An initial guess, a reference torus, $[\overline{\mathbf{x}}, \overline{Q}]$. Usually, we do not require the smooth torus itself, but rather just a δ-grid with δ sufficiently small, denoted $[\overline{\mathbf{x}}_{i_1,i_2,\ldots,i_p}, \overline{Q}_{i_1,i_2,\ldots,i_p}]$. In the continuation process, this is commonly either a known approximation from a previous λ value, or else a suitable correction of such.
(ii) A box scheme for determining instantaneous normal vectors, typically (20), (21), or (23).

These two items define the $qN_1N_2\cdots N_p$ equations (19) which we will solve by Newton's method for the unknown $(\mathbf{r}_{1,1,\ldots,1}, \mathbf{r}_{1,1,\ldots,2}, \ldots, \mathbf{r}_{N_1,N_2,\ldots,N_p})$.

Remark 3.1. It is natural to ask why consider the box scheme and not other (nominally second order) discretizations? Indeed, the box scheme seems more complicated than, say, centered differences. Alas, we have tried center- and directional-difference schemes without much success. Probably, the reason for the observed instability of center

differences is similar to the reason for instability of the scheme of [10]. Indeed, as mentioned in Remark 2.1, any discretization of the orthogonality condition generates a complementary discretization of the PDE (5) and a center-difference approximation is a notoriously unstable choice.

4. Stability and consistency for periodic orbits

In the case of a periodic orbit, the strategy for proving stability is the same as for proving stability of numerical schemes for two-point boundary value problems; in fact, we use the same setup as in [2, Section 5.2.2], to which we refer for the overall theory.

We will prove that the discrete equations (19) admit an isolated solution by showing that the Jacobian of the equations is non-singular when evaluated at the exact periodic solution (assumed to exist). In turn, the strategy for proving non-singularity of the Jacobian is to compare its block elements to the Fréchet derivative of a similar continuous problem, which will admit an isolated solution when certain (natural) conditions are satisfied. Consistency and second-order convergence will come directly from a comparison to the midpoint collocation discretization.

Remark 4.1. Although the overall strategy for showing convergence is standard, in the literature we have not found such arguments for precisely our problem. For this reason, we decided to give some details.

A hyperbolic[1] periodic solution of $\dot{\mathbf{x}} = \mathbf{\Phi}(\mathbf{x})$ satisfies the boundary value problem

$$\begin{aligned} &\dot{\mathbf{x}} = \tau\mathbf{\Phi}(\mathbf{x}), && 0 \leqslant t \leqslant 1,\\ &\dot{\tau} = 0,\\ &\mathbf{x}(1) - \mathbf{x}(0) = \mathbf{0},\\ &\sigma(\mathbf{x}) = 0, \end{aligned} \tag{24}$$

where τ is the (unknown) period, and σ is a scalar phase condition that makes the problem well-posed, so that the periodic orbit is a regular solution of (24). We will consider the following "classical choice" for σ. Let $\bar{\mathbf{x}}_1$ be a point on a reference curve, and let $\bar{\mathbf{x}}_1'$ represent differentiation with respect to ϕ. Then we consider

$$\sigma(\mathbf{x}) \equiv (\mathbf{x}(0) - \bar{\mathbf{x}}_1)^{\mathrm{T}}\bar{\mathbf{x}}_1', \tag{25}$$

with the understanding that $\mathbf{x}(0)$ is at the minimum distance from $\bar{\mathbf{x}}_1$. Using this in (24) ensures that a hyperbolic, periodic solution $\mathbf{x}^*(t)$, of period τ^*, will be a regular solution of (24) if $\mathbf{\Phi}(\mathbf{x}^*(0))^{\mathrm{T}}\bar{\mathbf{x}}_1' \neq 0$; the proof of this result is in [19]. Notice that the requirement $\mathbf{\Phi}(\mathbf{x}^*(0))^{\mathrm{T}}\bar{\mathbf{x}}_1' \neq 0$ is certainly satisfied if (3) holds.

Now take N points, $\bar{\mathbf{x}}_i$, (ordered with respect to ϕ) on the reference curve, and let $\bar{\mathbf{x}}_i'$ be the values of their derivatives with respect to ϕ, $i = 1, \ldots, N$. Let the periodic orbit $\mathbf{x}^*$ be parameterized by $\bar{\mathbf{x}}$ through (3), and assume that $\mathbf{x}^*|_{t=0}$ is the closest point to $\bar{\mathbf{x}}_1$. Then the problem

$$\begin{aligned} &\dot{\mathbf{x}} = \tau\mathbf{\Phi}(\mathbf{x}), && 0 \leqslant t \leqslant 1,\\ &\dot{t}_i = 0, && i = 1, 2, \ldots, N,\\ &\mathbf{x}(1) - \mathbf{x}(0) = \mathbf{0}\\ &(\mathbf{x}(t_i) - \bar{\mathbf{x}}_i)^{\mathrm{T}}\bar{\mathbf{x}}_i' = 0, && i = 1, \ldots, N, \end{aligned} \tag{26}$$

where τ and $0 < t_2 < \cdots < t_N < 1$ are unknowns, admits the periodic orbit $\mathbf{x}^*$ of period τ^* and uniquely defined values $0 = t_1, t_2, \ldots, t_N$, as an isolated solution. (This is because the periodic solution $\mathbf{x}^*$ satisfies (26) for uniquely defined $t_2, \ldots, t_N$, and is an isolated solution of (24)–(25).) Observe that in (26) rather than the values τ and $t_2, \ldots, t_N$, we can identify the unknowns also with the quantities

$$\mu^i := \tau(t_{i+1} - t_i), \quad \text{or} \quad \mu^i := \tau h_i, \quad h_i := t_{i+1} - t_i, \quad i = 1, \ldots, N, \tag{27}$$

[1] The simple characteristic multiplier 1 is the only multiplier on the unit circle.

with the usual constraints $t_1 = 0$ and $t_{N+1} = 1$. So doing, we can rewrite (26) as the following $N(n+1)$ boundary value problem:

$$\begin{aligned} &\dot{\mathbf{x}}^i = \mu^i \boldsymbol{\Phi}(\mathbf{x}^i), \qquad 0 \leqslant t \leqslant 1, \\ &\dot{\mu}^i = 0, \\ &\mathbf{x}^i(1) - \mathbf{x}^{i+1}(0) = \mathbf{0}, \\ &(\mathbf{x}^i(0) - \overline{\mathbf{x}}_i)^{\mathrm{T}} \overline{\mathbf{x}}_i' = 0. \end{aligned} \tag{28}$$

With these preparations, we can now state the following proposition.

Proposition 6. *Let* $\mathbf{x}^*$ *be a hyperbolic periodic solution of* (1), *isolated in a tubular neighborhood, and let* $\boldsymbol{\Phi}$ *be* $\mathscr{C}^2$ *with a Lipschitz condition on the second derivative in that neighborhood. Then for any reference curve* $[\overline{\mathbf{x}}, \overline{Q}]$ *that is equipped with a box scheme and parameterizes* $\mathbf{x}^*$ *through* (3), *there exists* $\delta > 0$ *such that for any* δ*-grid there exists a unique solution of* (19).

Proof. The $N(n-1)$ system of equations (19) has a solution if and only if the following $N(n+1)$ system does:

$$\begin{aligned} &\mathbf{x}_{i+1} - \mathbf{x}_i - \mu_i \boldsymbol{\Phi}((\mathbf{x}_{i+1} + \mathbf{x}_i)/2) = \mathbf{0}, \quad i = 1, 2, \ldots, N, \\ &(\mathbf{x}_i - \overline{\mathbf{x}}_i)^{\mathrm{T}} \overline{\mathbf{x}}_i' = 0. \end{aligned} \tag{29}$$

Thus, it suffices to show that the Jacobian of (29) is invertible when evaluated at the periodic orbit under the closeness conditions of the statement of the proposition. With respect to the ordering, $\{\mathbf{x}_1, \mathbf{x}_2, \ldots, \mathbf{x}_N, \mu_1, \mu_2, \ldots, \mu_N\}$ the Jacobian is

$$J = \begin{pmatrix} A & B \\ C & 0 \end{pmatrix}, \tag{30}$$

where

$$A = \begin{pmatrix} E_1 & F_1 & 0 & \cdots & 0 \\ 0 & E_2 & F_2 & \cdots & 0 \\ \vdots & \vdots & \vdots & \ddots & \vdots \\ F_N & 0 & 0 & \cdots & E_N \end{pmatrix}, \tag{31}$$

$$B = \begin{pmatrix} -\boldsymbol{\Phi}(\mathbf{x}_{1/2}) & 0 & \cdots & 0 \\ 0 & -\boldsymbol{\Phi}(\mathbf{x}_{2/2}) & \cdots & 0 \\ \vdots & \vdots & \ddots & \vdots \\ 0 & 0 & \cdots & -\boldsymbol{\Phi}(\mathbf{x}_{N/2}) \end{pmatrix}, \tag{32}$$

$$C = \begin{pmatrix} (\overline{\mathbf{x}}_1')^{\mathrm{T}} & 0 & \cdots & 0 \\ 0 & (\overline{\mathbf{x}}_2')^{\mathrm{T}} & \cdots & 0 \\ \vdots & \vdots & \ddots & \vdots \\ 0 & 0 & \cdots & (\overline{\mathbf{x}}_N')^{\mathrm{T}} \end{pmatrix}, \tag{33}$$

and we have used the following notation to condense the equations:

$$E_i = -\left(I + \frac{\mu_i}{2} D\boldsymbol{\Phi}(\mathbf{x}_{i/2})\right), \tag{34}$$

$$F_i = \left(I - \frac{\mu_i}{2} D\boldsymbol{\Phi}(\mathbf{x}_{i/2})\right), \tag{35}$$

and

$$\mathbf{x}_{i/2} = (\mathbf{x}_i + \mathbf{x}_{i+1})/2. \tag{36}$$

Left-multiplying the Jacobian by

$$G = \begin{pmatrix} -F_1^{-1} & 0 & \cdots & 0 & 0 \\ 0 & -F_2^{-1} & \cdots & 0 & 0 \\ \vdots & \vdots & \ddots & \vdots & \vdots \\ 0 & 0 & \cdots & -F_N^{-1} & 0 \\ 0 & 0 & \cdots & 0 & I \end{pmatrix} \tag{37}$$

gives

$$J' := GJ = \begin{pmatrix} A' & B' \\ C & 0 \end{pmatrix}, \tag{38}$$

where

$$A' = \begin{pmatrix} -F_1^{-1}E_1 & -I & 0 & \cdots & 0 \\ 0 & -F_2^{-1}E_2 & -I & \cdots & 0 \\ \vdots & \vdots & \vdots & \ddots & \vdots \\ -I & 0 & 0 & \cdots & -F_N^{-1}E_N \end{pmatrix}, \tag{39}$$

and

$$B' = \begin{pmatrix} F_1^{-1}\boldsymbol{\Phi}(\mathbf{x}_{1/2}) & 0 & \cdots & 0 \\ 0 & F_2^{-1}\boldsymbol{\Phi}(\mathbf{x}_{2/2}) & \cdots & 0 \\ \vdots & \vdots & \ddots & \vdots \\ 0 & 0 & \cdots & F_N^{-1}\boldsymbol{\Phi}(\mathbf{x}_{N/2}) \end{pmatrix}. \tag{40}$$

We note for future reference that, referring to (34)–(36), one has

$$-F_i^{-1}E_i = \exp(\mu_i D\boldsymbol{\Phi}(\mathbf{x}_{i/2})) + \mathrm{O}(\mu_i^2). \tag{41}$$

Under the assumptions of the proposition, the system in (28) has an isolated solution, denoted, $\{\mathbf{x}^i, \mu^i\}$, that corresponds to the periodic orbit in (1). We will show that J' evaluated at this solution is invertible by comparing it to the Fréchet derivative around the solution of (28).

Taking the perturbations, $\mathbf{x}^i \to \mathbf{x}^i + \mathbf{y}^i$ and $\mu^i \to \mu^i + v^i$, around the solution, the equations (28) leave a residue of

$$\mathbf{y}^{i+1}(0) - \mathbf{y}^i(1) \quad \text{and} \quad (\overline{\mathbf{x}}_i')^{\mathrm{T}}\mathbf{y}^i(0), \tag{42}$$

with the stipulation that

$$\dot{\mathbf{y}}^i = \mu^i D\boldsymbol{\Phi}(\mathbf{x}^i)\mathbf{y}^i + v^i\boldsymbol{\Phi}(\mathbf{x}^i). \tag{43}$$

Applying the variation of constants formula to (43) gives

$$\mathbf{y}^i(t) = Y^i(t)\left[\mathbf{y}^i(0) + v^i\int_0^t (Y^i(s))^{-1}\boldsymbol{\Phi}(\mathbf{x}^i)\,\mathrm{d}s\right], \tag{44}$$

where $Y^i(t)$ is the principal matrix solution of

$$\dot{\mathbf{y}}^i = \mu^i D\boldsymbol{\Phi}(\mathbf{x}^i)\mathbf{y}^i, \tag{45}$$

that is, for $i = 1, 2, \ldots, N$,

$$Y^i(0) = I$$

and

$$\dot{Y}^i = \mu^i D\boldsymbol{\Phi}(\mathbf{x}^i(t))Y^i, \quad 0 \leqslant t \leqslant 1. \tag{46}$$

It is now possible to write down the Fréchet derivative. The unknowns are $\{\mathbf{y}^i(0), v^i\}$, and combining (44) into (42) gives the matrix

$$T = \begin{pmatrix} L & M \\ C & 0 \end{pmatrix}, \tag{47}$$

where C is the same as in (33),

$$L = \begin{pmatrix} Y^1(1) & -I & 0 & \cdots & 0 \\ 0 & Y^2(1) & -I & \cdots & 0 \\ \vdots & \vdots & \vdots & \ddots & \vdots \\ -I & 0 & 0 & \cdots & Y^N(1) \end{pmatrix}, \tag{48}$$

and

$$M = \begin{pmatrix} P_1 & 0 & \cdots & 0 \\ 0 & P_2 & \cdots & 0 \\ \vdots & \vdots & \ddots & \vdots \\ 0 & 0 & \cdots & P_N \end{pmatrix} \quad \text{where } P_i = Y^i(1) \int_0^1 (Y^i(s))^{-1} \mathbf{\Phi}(\mathbf{x}^i(s))\, \mathrm{d}s. \tag{49}$$

It remains to be shown that the blocks of T and J' approach each other in matrix norm as $\delta \to 0$ for any reference curve sufficiently close to the actual orbit. We may assume that J' is evaluated at the points of the periodic orbit, so $\mathbf{x}_i = \mathbf{x}^i(0)$ and $\mu_i = \mu^i$. Because of the bound on the second derivative of the vector field in the assumptions of the proposition, δ must be of the same order as μ^i, and $\mathbf{x}_{i/2} = \mathbf{x}^i(1/2) + \mathrm{O}(\delta^2)$. Therefore, it suffices to show that the blocks of A' and B' converge toward the corresponding blocks of L and M, respectively. The first fact is simple, since (41) implies that

$$\|Y^i(1) - \exp(\mu^i D\mathbf{\Phi}(\mathbf{x}^i(1/2)))\| = \mathrm{O}(\delta^2). \tag{50}$$

Next, we examine

$$P_i - \left(I - \frac{\mu^i}{2} D\Phi(\mathbf{x}^i(1/2))\right)^{-1} \Phi(\mathbf{x}^i(1/2)).$$

Another way to write P_i is

$$\begin{aligned} P_i &= Y^i(1)(Y^i(1/2))^{-1}\mathbf{\Phi}(\mathbf{x}^i(1/2)) + \mathrm{O}(\delta^2) \\ &= Y^i(1, 1/2)\mathbf{\Phi}(\mathbf{x}^i(1/2)) + \mathrm{O}(\delta^2), \end{aligned} \tag{51}$$

where $Y^i(1, 1/2)$ is the solution at 1 of the linearized problem on $1/2 \leqslant t \leqslant 1$ with initial condition the identity at $t = 1/2$. Therefore,

$$Y^i(1, 1/2) = \left(I - \frac{\mu^i}{2} D\Phi(\mathbf{x}^i(1/2))\right)^{-1} + \mathrm{O}(\delta^2), \tag{52}$$

and the result follows. □

There are obvious parallels between scheme in (29) and the midpoint collocation discretization for the boundary-value problem (24). In particular, for mesh points $0 = t_1 < t_2 < \cdots < t_N < 1 = t_{N+1}$, with step sizes $h_i = t_{i+1} - t_i$, $i = 1, \ldots, N$, the midpoint collocation equations for (24)–(25) are

$$\begin{aligned} &\widehat{\mathbf{x}}_{i+1} - \widehat{\mathbf{x}}_i - \tau h_i \mathbf{\Phi}((\widehat{\mathbf{x}}_{i+1} + \widehat{\mathbf{x}}_i)/2) = \mathbf{0}, \qquad i = 1, 2, \ldots, N, \\ &(\widehat{\mathbf{x}}_1 - \overline{\mathbf{x}}_1)^{\mathrm{T}} \overline{\mathbf{x}}'_1 = 0. \end{aligned} \tag{53}$$

As a consequence of general results [2] for the collocation solution of (53) we have

$$\|\widehat{\mathbf{x}}_i - \mathbf{x}^*(t_i)\| = \mathrm{O}(h^2), \quad i = 1, 2, \ldots, N, \tag{54}$$

and

$$|\hat{\tau} - \tau^*| = \mathrm{O}(h^2), \tag{55}$$

where $h = \max_{1 \leqslant i \leqslant N} h_i$. This leads directly to consistency results for methods based on the orthogonality condition, according to the following proposition.

Proposition 7. *Let* $\mathbf{x}^*$ *be a hyperbolic, periodic solution of* (1) *that is isolated in a tubular neighborhood of radius* ρ_0, *and let* $\mathbf{\Phi}$ *be* $\mathscr{C}^2$ *with a Lipschitz condition on the second derivative in that neighborhood. Let* $[\overline{\mathbf{x}}, \overline{Q}]$ *be a reference curve that is equipped with a box scheme and parameterizes* $\mathbf{x}^*$ *through* (3). *Then the solution* $\{\widehat{\mathbf{x}}_i\}$ *to* (19) *satisfies*

$$\|\widehat{\mathbf{x}}_i - \overline{\mathbf{x}}_i\| = \mathrm{O}(\delta^2). \tag{56}$$

Proof. We note that a set of points $\widehat{\mathbf{x}}_i = \overline{\mathbf{x}}_i + \overline{Q}_i \mathbf{r}_i$ satisfies (19) with a non-vanishing vector field if and only if it satisfies (53) with

$$\tau(t_{i+1} - t_i) = \tau h_i = \|\widehat{\mathbf{x}}_{i+1} - \widehat{\mathbf{x}}_i\| / \|\mathbf{\Phi}((\widehat{\mathbf{x}}_{i+1} + \widehat{\mathbf{x}}_i)/2)\|. \tag{57}$$

Since the vector field is bounded above and below in norm, these quantities are of order δ, so (54) implies the proposition. □

Regretfully, the above argument applies neither to higher-dimensional tori nor to closed curves with equilibria (e.g., heteroclinic cycles). In fact, the method is generally unstable when applied directly to cycles with equilibria. One can nevertheless use the orthogonality condition to continue heteroclinic and homoclinic orbits, but it requires local departures from the box scheme—for example, individual tracking of the equilibria, coupled with a center-difference rule for the tangents, as in [25].

This leads to a natural question: what is the extension of this difficulty to the general case of a p-torus? Numerical experiments indicate that any closed invariant sub-manifold can induce instabilities in methods based on the orthogonality condition equipped with generalizations of the box scheme; we highlight this in Section 6, where we also give some indications of how to avoid this difficulty in practice.

5. Difficulties in higher dimensions

As mentioned in the "Introduction", the method can fail in two specific circumstances. One problem is the existence of invariant sub-manifolds such as periodic orbits or fixed points. The other problem, which we analyze first, is when more than one of the discretization numbers, $N_1, N_2, \ldots, N_p$, is even. Below, we show specifically that if the sought-after torus is a 2-torus in $\mathbb{R}^3$—and thus the box scheme is (21)—the Jacobian of the discrete system becomes arbitrarily ill-conditioned when both N_1 and N_2 are even.

From a practical standpoint, the fix for the second problem is simple and effective—we use odd numbers of discretization points in all directions. It is nevertheless instructive to delve intuitively and formally into the reasons why parity matters to the scheme.

5.1. Even–even discretizations of 2-Tori in $\mathbb{R}^3$

The geometrical explanation for how the method can fail with even–even discretizations relies on the fact that the approximate tangent vectors are not tied strongly to their locations. Consider, for example, a box consisting of four coplanar points. If we lift two opposite diagonal points above the plane by a certain amount and drop the other two below the plane by the same amount, then neither the average of the points nor the cross-product of the normalized tangents will change. Thus, the equation for that box is satisfied for many different configurations.

Globally, this does not present a problem unless one uses even numbers of points in both directions. To see why this creates a problem, we consider the points on the torus laid out in a square with the standard top/bottom, left/right identification. By lifting every other point (i.e., every other diagonal) and dropping the remaining points, it is possible to alter the torus without disturbing the discrete equations. If the grid has an odd number of points in either the vertical or horizontal direction, however, it is impossible to lift the diagonals uniformly without violating a boundary identification.

More formally, the Jacobian of an even–even discretization admits eigenvectors with increasingly small eigenvalues as the grid becomes more regular, a fact which we now prove.

Consider a reference 2-torus with a grid, $[\overline{\mathbf{x}}_{i,j}, \overline{\mathbf{n}}_{i,j}]$, embedded in $\mathbb{R}^3$. Combining (19) and (21) with the tangent vector formulation of (14) yields a set of $N_1 N_2$ equations,

$$f_{i,j} = 0, \quad i = 1, \ldots, N_1, \quad j = 1, \ldots, N_2 \tag{58}$$

where

$$f_{i,j} = \boldsymbol{\Phi}(\widetilde{\mathbf{x}})^{\mathrm{T}} \frac{(\widehat{\mathbf{x}}_{i+1,j+1} - \widehat{\mathbf{x}}_{i,j}) \times (\widehat{\mathbf{x}}_{i+1,j} - \widehat{\mathbf{x}}_{i,j+1})}{\|(\widehat{\mathbf{x}}_{i+1,j+1} - \widehat{\mathbf{x}}_{i,j}) \times (\widehat{\mathbf{x}}_{i+1,j} - \widehat{\mathbf{x}}_{i,j+1})\|}.$$

In (58), $\widetilde{\mathbf{x}}$ is the average at the vertices of the box:

$$\widetilde{\mathbf{x}} = (\widehat{\mathbf{x}}_{i,j} + \widehat{\mathbf{x}}_{i+1,j} + \widehat{\mathbf{x}}_{i,j+1} + \widehat{\mathbf{x}}_{i+1,j+1})/4. \tag{59}$$

Since the update vector $\mathbf{r} = (r_{1,1} \;\; r_{1,2} \;\; \cdots \;\; r_{N_1,N_2})^{\mathrm{T}}$ is related to the update through $\widehat{\mathbf{x}}_{i,j} = \overline{\mathbf{x}}_{i,j} + r_{i,j}\overline{\mathbf{n}}_{i,j}$, the unknown in (58) is simply $\mathbf{r}$. To simplify notation, let $\widetilde{\mathbf{n}}$ denote the cross-product quotient in (58).

Applying Newton's method to (58) leads to a matrix that is *block*, *periodic*, *bi-diagonal* with *periodic*, *bi-diagonal blocks*. In other words, the sparsity pattern of the Jacobian is

$$J = \begin{pmatrix} A_1 & B_1 & 0 & \cdots & 0 & 0 \\ 0 & A_2 & B_2 & \cdots & 0 & 0 \\ \vdots & \vdots & \vdots & \ddots & \vdots & \vdots \\ 0 & 0 & 0 & \cdots & A_{N_1-1} & B_{N_1-1} \\ B_{N_1} & 0 & 0 & \cdots & 0 & A_{N_1} \end{pmatrix}, \tag{60}$$

where each A_i and B_i is an $N_2 \times N_2$ periodic, bi-diagonal matrix (i.e., the same structure as J but with scalar blocks). Each row of the Jacobian has four non-zero entries:

$$\begin{aligned}
(A_i)_{j,j} &= \frac{\partial f_{i,j}}{\partial r_{i,j}} = \widetilde{\mathbf{n}}^{\mathrm{T}} D\boldsymbol{\Phi}(\widetilde{\mathbf{x}}) \frac{\overline{\mathbf{n}}_{i,j}}{4} + \boldsymbol{\Phi}(\widetilde{\mathbf{x}})^{\mathrm{T}} \frac{\partial \widetilde{\mathbf{n}}}{\partial r_{i,j}}, \\
(A_i)_{j,j+1} &= \frac{\partial f_{i,j}}{\partial r_{i,j+1}} = \widetilde{\mathbf{n}}^{\mathrm{T}} D\boldsymbol{\Phi}(\widetilde{\mathbf{x}}) \frac{\overline{\mathbf{n}}_{i,j+1}}{4} + \boldsymbol{\Phi}(\widetilde{\mathbf{x}})^{\mathrm{T}} \frac{\partial \widetilde{\mathbf{n}}}{\partial r_{i,j+1}}, \\
(B_i)_{j,j} &= \frac{\partial f_{i,j}}{\partial r_{i+1,j}} = \widetilde{\mathbf{n}}^{\mathrm{T}} D\boldsymbol{\Phi}(\widetilde{\mathbf{x}}) \frac{\overline{\mathbf{n}}_{i+1,j}}{4} + \boldsymbol{\Phi}(\widetilde{\mathbf{x}})^{\mathrm{T}} \frac{\partial \widetilde{\mathbf{n}}}{\partial r_{i+1,j}},
\end{aligned} \tag{61}$$

and

$$(B_i)_{j,j+1} = \frac{\partial f_{i,j}}{\partial r_{i+1,j+1}} = \widetilde{\mathbf{n}}^{\mathrm{T}} D\boldsymbol{\Phi}(\widetilde{\mathbf{x}}) \frac{\overline{\mathbf{n}}_{i+1,j+1}}{4} + \boldsymbol{\Phi}(\widetilde{\mathbf{x}})^{\mathrm{T}} \frac{\partial \widetilde{\mathbf{n}}}{\partial r_{i+1,j+1}}.$$

We now show that if N_1 and N_2 are both even, then the Jacobian generally becomes ill-conditioned. A technical proposition helps to establish this.

Proposition 8. *Let* $[\overline{\mathbf{x}}, \overline{\mathbf{n}}]$ *be a reference torus, and let* $\widetilde{\mathbf{n}}$ *be the cross-product quotient in* (58) (*used in* (61)). *Then, for any* $\varepsilon > 0$, *there exist* $\alpha, \delta > 0$ *such that for any* δ*-grid,* $[\overline{\mathbf{x}}_{i,j}, \overline{\mathbf{n}}_{i,j}]$, *and for any* α*-update,* $\{r_{i,j}\}$,

$$\left\| \frac{\partial \widetilde{\mathbf{n}}}{\partial r_{i+1,j+1}} + \frac{\partial \widetilde{\mathbf{n}}}{\partial r_{i,j}} \right\| < \varepsilon \quad \textit{and} \quad \left\| \frac{\partial \widetilde{\mathbf{n}}}{\partial r_{i+1,j}} + \frac{\partial \widetilde{\mathbf{n}}}{\partial r_{i,j+1}} \right\| < \varepsilon, \tag{62}$$

for all $i = 1, 2, \ldots, N_1$, $j = 1, 2, \ldots, N_2$.

Proof. We concentrate on the first inequality in (62) because the proof of the second is essentially identical. Recall the definitions of $\widehat{\mathbf{x}}_{-}^{(1,2)}$ in (14), where with $\widehat{\mathbf{x}}_{-}^{(1,2)}$ we indicate either of $\widehat{\mathbf{x}}_{-}^{(1)}$ or $\widehat{\mathbf{x}}_{-}^{(2)}$, and let $\overline{\mathbf{x}}_{-}^{(1,2)}$ and $\overline{\mathbf{n}}_{-}^{(1,2)}$ be the natural analogs; e.g., $\overline{\mathbf{n}}_{-}^{(1)} = (\overline{\mathbf{n}}_{i+1,j+1} - \overline{\mathbf{n}}_{i,j})$.

We write the sum of derivatives as

$$\frac{\partial \widetilde{\mathbf{n}}}{\partial r_{i+1,j+1}} + \frac{\partial \widetilde{\mathbf{n}}}{\partial r_{i,j}} = \frac{\overline{\mathbf{n}}_-^{(1)} \times \widehat{\mathbf{x}}_-^{(2)}}{\|\widehat{\mathbf{x}}_-^{(1)} \times \widehat{\mathbf{x}}_-^{(2)}\|} - \frac{(\widehat{\mathbf{x}}_-^{(1)} \times \widehat{\mathbf{x}}_-^{(2)})(\widehat{\mathbf{x}}_-^{(1)} \times \widehat{\mathbf{x}}_-^{(2)})^{\mathrm{T}}}{\|\widehat{\mathbf{x}}_-^{(1)} \times \widehat{\mathbf{x}}_-^{(2)}\|^3}(\overline{\mathbf{n}}_-^{(1)} \times \widehat{\mathbf{x}}_-^{(2)}), \tag{63}$$

or more compactly as

$$\frac{\partial \widetilde{\mathbf{n}}}{\partial r_{i+1,j+1}} + \frac{\partial \widetilde{\mathbf{n}}}{\partial r_{i,j}} = \Pi_{\mathscr{T}} \frac{\overline{\mathbf{n}}_-^{(1)} \times \widehat{\mathbf{x}}_-^{(2)}}{\|\widehat{\mathbf{x}}_-^{(1)} \times \widehat{\mathbf{x}}_-^{(2)}\|}, \tag{64}$$

where $\Pi_{\mathscr{T}}$ is the projection onto the "tangent space at the half point": the span of $\widehat{\mathbf{x}}_-^{(1)}$ and $\widehat{\mathbf{x}}_-^{(2)}$. The two-part strategy for minimizing this projection is (1) show that the item being projected is bounded in norm, and then (2) show that it approaches the normal direction, and thus that the norm of the projection goes to zero by restricting α and δ.

First, we find a lower bound on the cross product in the denominator in (64). Let $\theta(\widehat{\mathbf{x}}_-^{(1,2)}, \overline{\mathbf{x}}_-^{(1,2)})$ denote the angle between the vectors $\widehat{\mathbf{x}}_-^{(1)}$ and $\overline{\mathbf{x}}_-^{(1)}$ or $\widehat{\mathbf{x}}_-^{(2)}$ and $\overline{\mathbf{x}}_-^{(2)}$, respectively, and a similar notation be adopted for angles between the other vectors.

By (18), we have $\theta(\widehat{\mathbf{x}}_-^{(1,2)}, \overline{\mathbf{x}}_-^{(1,2)}) > \cos^{-1}(1-\alpha)$. By (15), we have $\theta(\overline{\mathbf{x}}_-^{(1)}, \overline{\mathbf{x}}_-^{(2)}) < \cos^{-1}(\delta)$. Therefore, since

$$\theta(\widehat{\mathbf{x}}_-^{(1)}, \widehat{\mathbf{x}}_-^{(2)}) \geqslant \theta(\overline{\mathbf{x}}_-^{(1)}, \overline{\mathbf{x}}_-^{(2)}) - \theta(\widehat{\mathbf{x}}_-^{(1)}, \overline{\mathbf{x}}_-^{(1)}) - \theta(\widehat{\mathbf{x}}_-^{(2)}, \overline{\mathbf{x}}_-^{(2)}),$$

we have that

$$\theta(\widehat{\mathbf{x}}_-^{(1)}, \widehat{\mathbf{x}}_-^{(2)}) > \cos^{-1}(\delta) - 2\cos^{-1}(1-\alpha). \tag{65}$$

This implies

$$\|\widehat{\mathbf{x}}_-^{(1)} \times \widehat{\mathbf{x}}_-^{(2)}\| > C\|\widehat{\mathbf{x}}_-^{(1)}\|\|\widehat{\mathbf{x}}_-^{(2)}\|, \tag{66}$$

where $C = \sin(\cos^{-1}(\delta) - 2\cos^{-1}(1-\alpha))$. Applying (17), we obtain the overall bound,

$$\frac{\|\overline{\mathbf{n}}_-^{(1)} \times \widehat{\mathbf{x}}_-^{(2)}\|}{\|\widehat{\mathbf{x}}_-^{(1)} \times \widehat{\mathbf{x}}_-^{(2)}\|} < \frac{\|\overline{\mathbf{n}}_-^{(1)} \times \widehat{\mathbf{x}}_-^{(2)}\|}{C(1-\alpha)\|\overline{\mathbf{x}}_-^{(1)}\|\|\widehat{\mathbf{x}}_-^{(2)}\|}. \tag{67}$$

We note that $\overline{\mathbf{n}}_-^{(1)}/\|\overline{\mathbf{x}}_-^{(1)}\|$ is a second-order approximation in δ to a derivative of the unit normal vector along the surface of the reference torus in the center of the box. Because the reference torus is $\mathscr{C}^2$ by assumption, this derivative is well-defined and finite and lies in the tangent space. It therefore suffices to show that the cross product,

$$(\overline{\mathbf{n}}_-^{(1)}/\|\overline{\mathbf{x}}_-^{(1)}\|) \times (\widehat{\mathbf{x}}_-^{(2)}/\|\widehat{\mathbf{x}}_-^{(2)}\|),$$

approaches the direction of $\widetilde{\mathbf{n}}$ as $\alpha, \delta \to 0$ (independently). The difference vectors $\overline{\mathbf{x}}_-^{(1)}$ and $\overline{\mathbf{x}}_-^{(2)}$ are themselves second-order approximations to tangent vectors, so for sufficiently small δ we may express the difference as

$$\frac{\overline{\mathbf{n}}_-^{(1)}}{\|\overline{\mathbf{x}}_-^{(1)}\|} = a\overline{\mathbf{x}}_-^{(1)} + b\overline{\mathbf{x}}_-^{(2)} + \mathrm{O}(\delta^2). \tag{68}$$

By (18), the angle between $\widehat{\mathbf{x}}_-^{(1,2)}$ and $\overline{\mathbf{x}}_-^{(1,2)}$ is of order α. This implies that

$$\frac{\overline{\mathbf{n}}_-^{(1)}}{\|\overline{\mathbf{x}}_-^{(1)}\|} = a\widehat{\mathbf{x}}_-^{(1)} + b\widehat{\mathbf{x}}_-^{(2)} + \mathrm{O}(\alpha) + \mathrm{O}(\delta^2), \tag{69}$$

and thus,

$$\Pi_{\mathscr{T}} \left(\frac{\overline{\mathbf{n}}_-^{(1)}}{\|\overline{\mathbf{x}}_-^{(1)}\|} \times \frac{\widehat{\mathbf{x}}_-^{(2)}}{\|\widehat{\mathbf{x}}_-^{(2)}\|} \right) = \mathrm{O}(\alpha) + \mathrm{O}(\delta^2), \tag{70}$$

which completes the proof. □

Proposition 8 explains why the Jacobian becomes arbitrarily ill-conditioned when N_1 and N_2 are even and α and δ are small. The difference between sub-blocks in (60) is

$$A_i - B_i = \begin{pmatrix} c_{i,1} & c_{i,1} & 0 & \cdots & 0 & 0 \\ 0 & c_{i,2} & c_{i,2} & \cdots & 0 & 0 \\ \vdots & \vdots & \vdots & \ddots & \vdots & \vdots \\ 0 & 0 & 0 & \cdots & c_{i,N_2-1} & c_{i,N_2-1} \\ c_{i,N_2} & 0 & 0 & \cdots & 0 & c_{i,N_2} \end{pmatrix} + \begin{pmatrix} \varepsilon_{i,1} & \varepsilon'_{i,1} & 0 & \cdots & 0 & 0 \\ 0 & \varepsilon_{i,2} & \varepsilon'_{i,2} & \cdots & 0 & 0 \\ \vdots & \vdots & \vdots & \ddots & \vdots & \vdots \\ 0 & 0 & 0 & \cdots & \varepsilon_{i,N_2-1} & \varepsilon'_{i,N_2-1} \\ \varepsilon'_{i,N_2} & 0 & 0 & \cdots & 0 & \varepsilon_{i,N_2} \end{pmatrix}, \tag{71}$$

where

$$c_{i,j} = \boldsymbol{\Phi}(\widetilde{\mathbf{x}})^{\mathrm{T}} \left(\frac{\partial \widetilde{\mathbf{n}}}{\partial r_{i,j}} - \frac{\partial \widetilde{\mathbf{n}}}{\partial r_{i+1,j}} \right), \tag{72}$$

$$\varepsilon_{i,j} = \widetilde{\mathbf{n}}^{\mathrm{T}} D\boldsymbol{\Phi}(\widetilde{\mathbf{x}}) \frac{\overline{\mathbf{n}}_{i,j} - \overline{\mathbf{n}}_{i+1,j}}{4} \tag{73}$$

and

$$\varepsilon'_{i,j} = \widetilde{\mathbf{n}}^{\mathrm{T}} D\boldsymbol{\Phi}(\widetilde{\mathbf{x}}) \frac{\overline{\mathbf{n}}_{i,j+1} - \overline{\mathbf{n}}_{i+1,j+1}}{4} + \boldsymbol{\Phi}(\widetilde{\mathbf{x}})^{\mathrm{T}} \left(\frac{\partial \widetilde{\mathbf{n}}}{\partial r_{i,j+1}} - \frac{\partial \widetilde{\mathbf{n}}}{\partial r_{i+1,j+1}} - \frac{\partial \widetilde{\mathbf{n}}}{\partial r_{i,j}} + \frac{\partial \widetilde{\mathbf{n}}}{\partial r_{i+1,j}} \right).$$

If N_2 is even, then the first matrix on the right-hand side of (71) has a null eigenvector:

$$\mathbf{v} = (1 \quad -1 \quad 1 \quad \cdots \quad -1)^{\mathrm{T}}. \tag{74}$$

Hence, if $\varepsilon_{i,j}, \varepsilon'_{i,j} = 0$ for all i, j, and if N_1 and N_2 are even, then the Jacobian is singular with a null eigenvector:

$$(\mathbf{v}^{\mathrm{T}} \quad -\mathbf{v}^{\mathrm{T}} \quad \mathbf{v}^{\mathrm{T}} \quad \cdots \quad -\mathbf{v}^{\mathrm{T}})^{\mathrm{T}}. \tag{75}$$

To show ill-conditioning, it therefore suffices to minimize all the $\varepsilon_{i,j}$ and $\varepsilon'_{i,j}$ using α and δ, which is a direct result of Proposition 8.

5.2. *Jacobian for general box schemes*

The above argument technically only works for 2-tori in $\mathbb{R}^3$. Still, numerical experiments in several dimensions have shown that box schemes with more than one even N_k tend to be unstable [25]. (Rigorously proving that even numbers induce multiple solutions in the general algorithm would be extremely complicated, since the cross product and its elegant derivative properties are not available.) Thus, the most obvious way to attempt to prevent ill-conditioning of the Jacobian is to force all but possibly one of $N_1, N_2, \ldots, N_p$ to be odd. Even this precaution will not guarantee stability for tori that contain closed, invariant sub-manifolds. To apply the method to such systems, one should either track the sub-manifolds individually and modify the box scheme with *a priori* information, or else ensure that the grid does not align with the sub-manifolds [25] in the sense that an ordered set of points on the grid lies entirely on or near a sub-manifold. In the next section we adopt the latter stabilization for an example of a 2-torus with periodic orbits embedded in $\mathbb{R}^4$.

The sparsity pattern of the Jacobian for a box scheme applied to a p-torus in $\mathbb{R}^n$ is well understood: The Jacobian is periodic, block bi-diagonal with periodic, block bi-diagonal blocks, and so on to p levels of nesting. The lowest (pth) structure is periodic, block, bi-diagonal with full $(q \times q)$ blocks. Fig. 1 illustrates the sparsity pattern of an example Jacobian for a $5 \times 5 \times 5$ three-torus in $\mathbb{R}^7$. The black boxes in the center of the plots indicate the region of magnification for the next plot, ordered left to right, top to bottom.

A matrix of this form potentially contains $q^2 2^p N_1 N_2 \cdots N_p$ non-zero elements, and thus the number of non-zero elements in the Jacobian grows rapidly with the dimension of both the ambient space and the torus itself. While some direct and iterative techniques are available for solving systems like these, both memory and computation time can be limitations [25]. Our computations in the next section are restricted to problems that are small enough to permit general purpose solution techniques of the resulting linear systems.

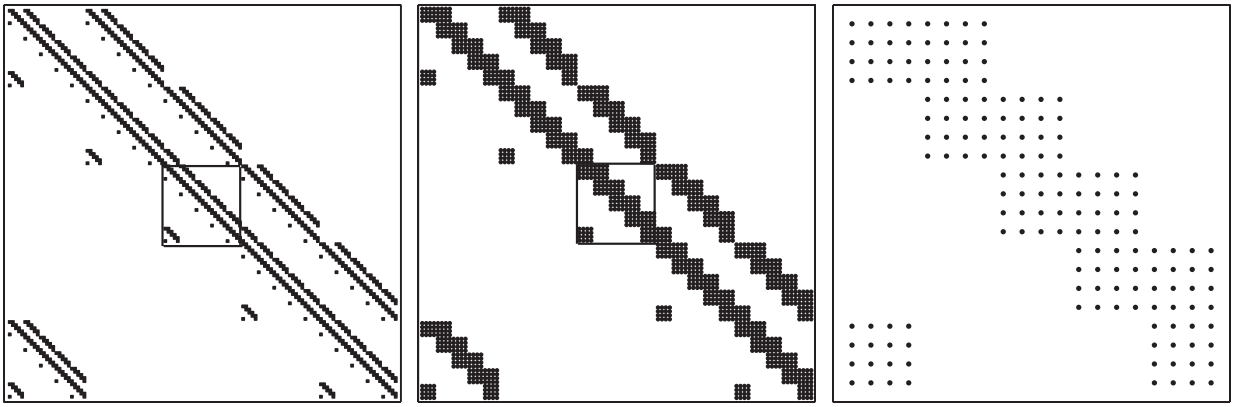

Fig. 1. Sparsity plot of Jacobian for $5 \times 5 \times 5$ Three-torus in $\mathbb{R}^7$.

6. Numerical results

With appropriate measures to cope with the difficulties explained above, the method is still attractive. We give several examples of periodic orbits and 2-tori embedded in real spaces of various dimension.

The first example is a periodic orbit in the forced van der Pol oscillator (a one-torus in $\mathbb{R}^3$). The next two examples are 2-tori embedded in $\mathbb{R}^3$. We compute a torus in the forced van der Pol oscillator that surrounds the aforementioned periodic orbit, and then we compute a sometimes-quasi-periodic 2-torus in a system of three equations that model an electrical circuit. Finally, we consider a pair of coupled oscillators that give rise to compute a 2-torus embedded in $\mathbb{R}^4$.

These examples test all modes of the algorithm and are common in the literature, which allows for comparison to other techniques.

6.1. Forced van der Pol oscillator

We first test the method by computing both a branch of periodic orbits and a branch of tori that arise in the *forced van der Pol oscillator* [15,16],

$$\ddot{x} + \alpha\dot{x}(x^2 - 1) + x = \lambda\cos(\omega\theta), \tag{76}$$

rewritten as the first-order system

$$\begin{aligned} \dot{x} &= y + \alpha x(1 - x^2/3), \\ \dot{y} &= -x + \lambda\cos(\omega\theta), \end{aligned} \tag{77}$$

where $\alpha > 0$, $\omega > 0$, and $\lambda\cos(\omega\theta)$ is the forcing term. It is well known that at $\lambda = 0$, the system has a unique attracting periodic orbit, a fixed point for the period map. For $\lambda > 0$, small, the period map has an invariant circle, an invariant torus for the original system. Computation of this torus has been done several times before, e.g., see [8,10,11,22,26,29,30], and thus the results we obtain can be cross-validated.

We add a trivial equation, $\dot{\theta} = 1$, plus a shift, $y \leftarrow y - 5$, to prevent the resulting invariant torus from overlapping itself. Finally, we let $x_1 = y\cos(\omega\theta)$, $x_2 = y\sin(\omega\theta)$, and $x_3 = x$, and rewrite the system as

$$\begin{aligned} \dot{x}_1 &= \lambda x_1^2 \Big/ (x_1^2 + x_2^2) - x_1 x_3 \Big/ \sqrt{x_1^2 + x_2^2} - \omega x_2, \\ \dot{x}_2 &= \lambda x_1 x_2 \Big/ (x_1^2 + x_2^2) - x_2 x_3 \Big/ \sqrt{x_1^2 + x_2^2} + \omega x_1, \\ \dot{x}_3 &= \sqrt{x_1^2 + x_2^2} - 5 + \alpha x_3(1 - x_3^2/3). \end{aligned} \tag{78}$$

We let $\alpha = 0.4$ and consider $\omega = \sqrt{0.84}$ and $\sqrt{0.78}$, which are standard parameter values in the previously cited literature.

The bifurcation diagram of the averaged system ([15, pp. 70–72], for example), along with the associated phase portraits, shows that for $\omega = \sqrt{0.84}$, the averaged system admits a source and a limit cycle from $\lambda = 0$ until $\lambda \approx 0.26$. Immediately above that value of λ, the source remains, but the limit cycle transforms into a sink and a saddle linked in a stable, closed heteroclinic cycle. This portrait persists until $\lambda \approx 0.35$, and then the entire system collapses into a single sink. In the full system, this sequence of bifurcations implies the existence of a repelling periodic orbit inside a torus from $\lambda = 0$ until $\lambda \approx 0.35$, when both the orbit and the torus break down simultaneously. (The bifurcation value of λ in the full system will not exactly match the 2-D calculation due to averaging.)

The sequence for $\omega = \sqrt{0.78}$ is somewhat more complicated. The averaged system still has a source and a limit cycle which bifurcates into a source and a closed, heteroclinic orbit at $\lambda \approx 0.37$. After that, however, the system sees several bifurcations in rapid succession until the whole system finally collapses into a sink at $\lambda \approx 0.39$. The most important event in that sequence is when the closed heteroclinic orbit breaks apart, so the saddle and sink are still connected, but only along a single line. This indicates the breakdown of the torus in the full system, while the periodic orbit (which now corresponds to the source) persists longer.

6.1.1. Periodic orbit in forced van der Pol

The first test of our method is the continuation of the periodic orbits in the forced van der Pol oscillator. We must first start with an initial guess. The initial approximation at $\lambda = 0$ is a set of points on the known location of the periodic orbit with known normal directions,

$$\bar{\mathbf{x}}_i = 5\begin{pmatrix}\cos\theta_i\\ \sin\theta_i\\ 0\end{pmatrix}, \quad \overline{Q}_i = \begin{pmatrix}\cos\theta_i & 0\\ \sin\theta_i & 0\\ 0 & 1\end{pmatrix}, \tag{79}$$

for $i = 1, 2, \ldots, N$ and evenly spaced values, $\theta_i = 2\pi(i-1)/N$.

With this reference curve in hand, we compute the branch of periodic orbits according to the following process:

(i) Generate the initial grid $\{\bar{\mathbf{x}}_i, \overline{Q}_i\}$, $i = 1, 2, \ldots, N$, for the initial λ. This gives $2N$ equations through (19) and (23). The $2N$ unknowns are $\{\mathbf{r}_i\}$, given through $\widehat{\mathbf{x}}_i = \bar{\mathbf{x}}_i + \overline{Q}_i \mathbf{r}_i$.
(ii) Solve these equations using Newton's method with a forward-difference Jacobian.
(iii) Upon convergence of Newton's method, the approximation of the curve is $\{\widehat{\mathbf{x}}_i\}$. Update the grid, $\{\bar{\mathbf{x}}_i\} \leftarrow \{\widehat{\mathbf{x}}_i\}$.
(iv) Re-distribute $\{\bar{\mathbf{x}}_i\}$ by linear arc-length with fixed $\bar{\mathbf{x}}_1$.
(v) Update the reference normal directions by performing the QR decomposition on the matrix $(\mathbf{t}_i \ \ \overline{Q}_i)$, where $\mathbf{t}_i = (\bar{\mathbf{x}}_{i+1} - \bar{\mathbf{x}}_{i-1})/\|\bar{\mathbf{x}}_{i+1} - \bar{\mathbf{x}}_{i-1}\|$. (Recall that we take R with positive diagonal.) The new matrix $\overline{Q}_i$ will be the last two columns of the orthogonal matrix resulting from such QR decomposition, just as in (23).
(v) Update λ and return to step (ii) with the new grid $\{\bar{\mathbf{x}}_i, \overline{Q}_i\}$ and its resulting equations defined through (19) and (23).

For our numerical experiments, we have used $N = 55$. The continuation step size starts at $\Delta\lambda = 0.1$, and then we divide the step size by 10 when the next λ step would drive the process past breakdown. For example, when $\omega = \sqrt{0.84}$, the breakdown point is $\lambda \approx 0.3416$, so we proceed from 0 to 0.3 in steps of 0.1, then to 0.34 in steps of 0.01, then from 0.3411 to 0.3415 in steps of 0.0001.

The method has been implemented in `Matlab` using its built-in functions for solving linear systems and estimating the 1-norm condition number. The Jacobian comes from forward differences on $\mathbf{r}$ and the convergence condition for the Newton process is that the 2-norm of the left-hand side of the system (19) be less than 10^{-4}. The Newton process converges quadratically throughout, and the Jacobians are well-conditioned along the branch. The condition numbers are about 100 at the beginning and remain relatively low for most of the continuation process. As λ approaches the breakdown values, the condition number grows to about 3.5×10^5 and 2.5×10^4 for $\omega = \sqrt{0.84}$ and $\sqrt{0.78}$, respectively.

Fig. 2 shows the periodic orbits. The curves for $\omega = \sqrt{0.84}$ are at $\lambda = 0$, 0.1, 0.2, 0.3, 0.34, 0.3410, and 0.3415. The curves for $\omega = \sqrt{0.78}$ are at $\lambda = 0$, 0.1, 0.2, 0.3, 0.35, 0.38, 0.39, and 0.3945. All curves show the computed orbit after convergence, but before arc-length redistribution.

We have used this method for several other periodic orbits, including some planar examples where we have taken advantage of the simple box scheme in (20). In our experience, the method is very robust, and its simplicity and low cost make it a possible alternative to existing techniques for the approximation of periodic orbits [25].

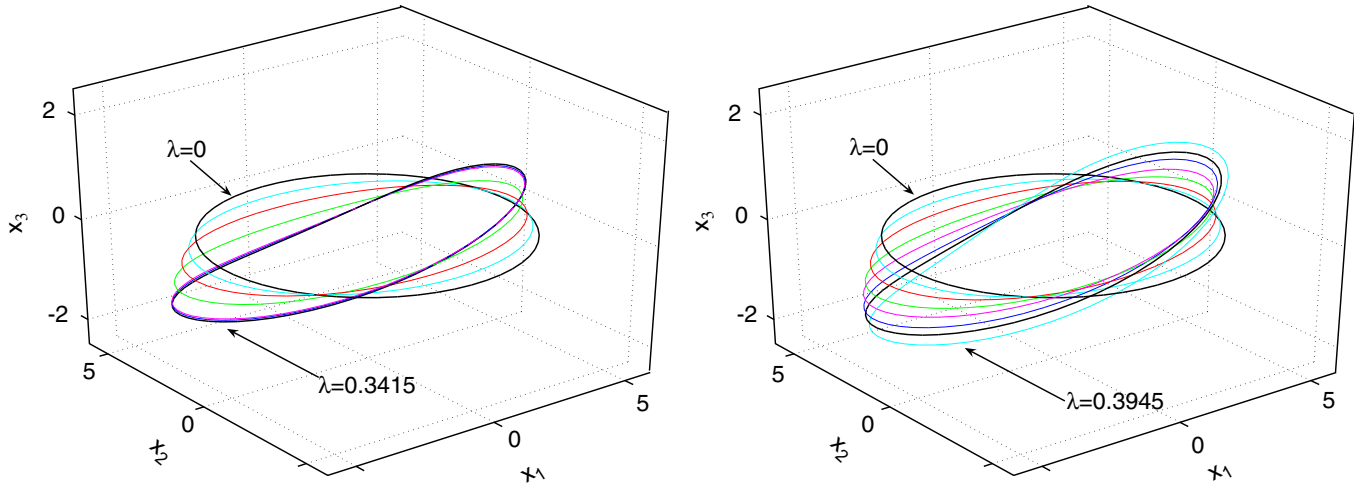

Fig. 2. Branch of periodic orbits; $\omega = \sqrt{0.84}$ (l), $\sqrt{0.78}$ (r).

6.1.2. Torus in forced van der Pol

The computation of the full 2-torus in the forced van der Pol oscillator is similar to the periodic orbit, except that here the cross-product is available to replace the more complicated "seeded QR decomposition," because the codimension in $\mathbb{R}^3$ of the torus is 1.

For both values of ω, the initial guess (guess, not solution) for an invariant torus at $\lambda = 0$ is

$$\bar{\mathbf{x}}((\phi_1)_i, (\phi_2)_j) = \bar{\mathbf{x}}_{i,j} = \begin{pmatrix} (5 + 2\cos(\phi_2)_j)\cos(\phi_1)_i \\ -(5 + 2\cos(\phi_2)_j)\sin(\phi_1)_i \\ 2\sin(\phi_2)_j \end{pmatrix}, \tag{80}$$

where $(\phi_1)_i = 2\pi(i-1)/N_1$ and $(\phi_1)_j = 2\pi(j-1)/N_2$.

The initial normal vectors are the cross-product of center differences. We calculate the Jacobian from forward-differencing on r. The cut-off criterion for Newton's method is that the 2-norm of the Newton's correction be less than 10^{-6}.

As with the periodic orbit, we begin with $\Delta\lambda = 0.1$ and reduce it by a factor of 10^{-1} when the next continuation step would be beyond the breakdown point. The final step size near breakdown in both cases is 10^{-4}. (We also resolve the torus for $\omega = \sqrt{0.84}$ at $\lambda = 0.3415$ in order to compare the torus to the periodic orbit near the breakdown of the orbit.)

When $\omega = \sqrt{0.84}$, we use $N_1 = N_2 = 45$, which leads to a 1-norm condition number estimate for the Jacobian of approximately 600 at first, increasing to 10^6 near breakdown. When $\omega = \sqrt{0.78}$, we set $N_1 = 105$ and $N_2 = 45$. The condition number is roughly the same as in the $\omega = \sqrt{0.84}$ case, except that the lowest values are approximately 1200 instead of 600.

Even though the code is in `Matlab` and is not completely vectorizable—it is impossible to avoid at least one loop over each column of the Jacobian—the sparsity of the Jacobian allows for relatively quick generation. On a 2.8 GHz Intel Pentium IV platform, each Newton step takes about 1 s for $N_1 = N_2 = 45$ and 5 s for $N_1 = 105$ and $N_2 = 45$. On average, each continuation step requires three Newton steps.

Figs. 3 and 4 show the results of the method applied to the van der Pol torus. The center line in each plot is the computed periodic orbit at that λ. In both pictures, the torus contorts and pinches as the continuation process moves to breakdown (c.f. [10,11,26]).

When $\omega = \sqrt{0.84}$, we are able to continue the torus numerically to $\lambda_{\max} = 0.3453$ but the periodic orbit only to 0.3415. As mentioned above, the bifurcation diagram for the averaged system at that value of ω suggests that the torus collapses in a saddle-node bifurcation of limit cycles at the same time as the periodic orbit. Numerical continuation of the periodic orbit using the standard package `AUTO` [9] verifies that the simultaneous collapse of the torus and periodic orbit occurs at $\lambda \approx 0.342$, which means that our method for invariant tori converges past the true breakdown point.[2]

[2] Thanks to one of the referees for suggesting and verifying the `AUTO` calculations in this paper.

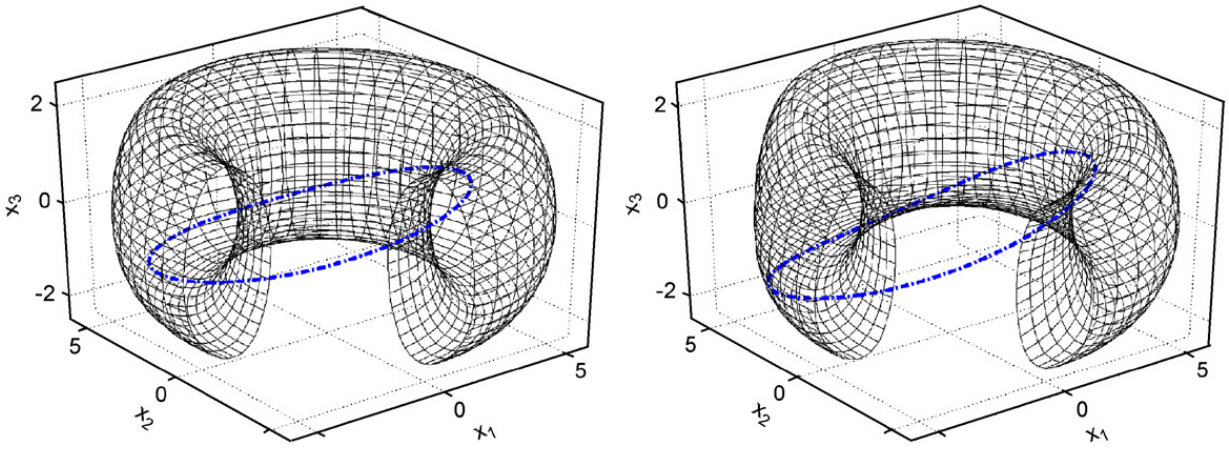

Fig. 3. Forced van der Pol torus with periodic orbit; $\omega = \sqrt{0.84}$, $\lambda = 0.3$ and 0.3415.

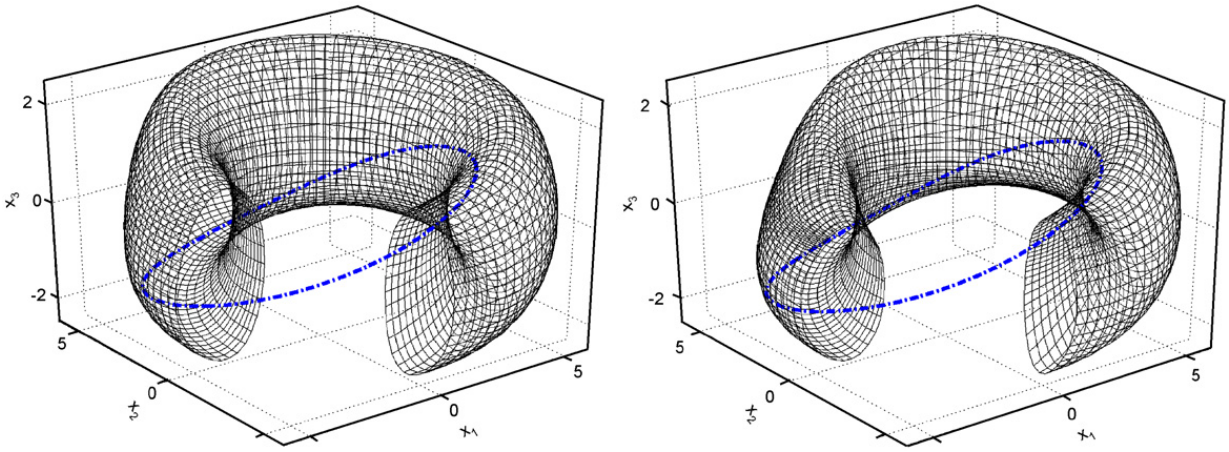

Fig. 4. Forced van der Pol torus with periodic orbit; $\omega = \sqrt{0.78}$, $\lambda = 0.38$ and 0.388.

This is often a limitation of manifold continuation methods in general—while the existence of an isolated manifold in many cases implies the convergence of the method, the converse is not always true. To determine the exact breakdown point, it is necessary to resort to other techniques, for example [20].

The breakdown mechanism for both the torus and the numerical method are more standard when $\omega = \sqrt{0.78}$. Continuation of the periodic orbit using AUTO shows that the torus is indeed destroyed in an reverse Neimark-Sacker bifurcation at $\lambda \approx 0.393$, just as the averaged system indicates. Our final point is $\lambda = 0.388$, which is close, albeit there is significant further distortion of the torus before breakdown. We are not able to continue closer to $\lambda = 0.393$ because the torus is distorting very quickly as it collapses into the periodic orbit, and thus the mesh is becoming very irregular.

More continuation with AUTO illuminates the progress of the periodic orbit immediately before and after the destruction of the torus. Before the destruction of the torus, at $\lambda \approx 0.391$, there is a saddle-node bifurcation of another periodic orbit into an attracting and saddle-type orbit. At the Neimark-Sacker bifurcation, the torus shrinks into the periodic orbit which we have been following, which thereafter changes stability from repelling to attracting. The (now attracting) orbit continues until it undergoes a saddle-node bifurcation at $\lambda \approx 0.395$ by colliding with the saddle orbit from the above-mentioned bifurcation. The final λ value computed with our method is 0.3945. We did not attempt to follow the orbit for decreasing λ after the fold because it has little to do with the breakdown of the torus itself.

6.2. Forced electrical circuit

The second example of a 2-torus in $\mathbb{R}^3$ results from a set of equations that describe voltage in an electrical circuit. This example is very similar in construction and philosophy to the forced van der Pol oscillator, and we include it here for comparison to the recent work [28].

The circuit is a parametrically forced RLC circuit with a time-dependent inductor and a cubic resistor. The voltage obeys a second-order equation, as explained in [28]. This equation is

$$\ddot{x} + (\lambda - B)\dot{x}^3 - (\lambda/2 - B) + (1 + B\sin 2t)x = 0, \tag{81}$$

where B is a scalar parameter and λ is the continuation parameter. This reduces to the first-order system,

$$\begin{aligned} \dot{x} &= y, \\ \dot{y} &= -(1 + B\sin 2t)x + (\lambda/2 - B)y - (\lambda - B)y^3. \end{aligned} \tag{82}$$

We replace time with a third variable, $\theta = 2t$, add the trivial equation $\dot{\theta} = 2$, and make a shift, $x \leftarrow x - 3$. Finally, we let $x_1 = x\cos(\theta)$, $x_2 = x\sin(\theta)$, and $x_3 = y$, and rewrite the system as

$$\begin{aligned} \dot{x}_1 &= x_1 x_3 \Big/ \sqrt{x_1^2 + x_2^2} - 2x_2, \\ \dot{x}_2 &= x_2 x_3 \Big/ \sqrt{x_1^2 + x_2^2} + 2x_1, \\ \dot{x}_3 &= -\sqrt{x_1^2 + x_2^2} + 3 + 3Bx_2 \Big/ \sqrt{x_1^2 + x_2^2} - Bx_2 + (\lambda/2 - B)x_3(\lambda - B)x_3^3. \end{aligned} \tag{83}$$

For comparison to [28], we let $B = 0.1$. For this value of B, the system admits a branch of quasi-periodic orbits with occasional resonance windows. We refer to [28] for a detailed discussion of the bifurcation diagram; there, it is seen that the 1:2 resonance tongue covers (approximately) $\lambda \in [0.3, 1.6]$; the 1:3 tongue covers $\lambda \in [7.0, 7.1]$, and the 1:4 tongue covers $\lambda \in [10.3, 12.8]$.

The method of [28] is limited to quasi-periodic tori, and the authors used it between the 1:2 and 1:3 tongues, from $\lambda = 1.7$ to $\lambda = 6.98$. The method we analyzed here is not designed solely for quasi-periodic tori, so we can consider the larger interval $\lambda \in [1.0, 12.8]$. The initial guess for the torus at $\lambda = 1.0$ is

$$\bar{\mathbf{x}}((\phi_1)_i, (\phi_2)_j) = \bar{\mathbf{x}}_{i,j} = \begin{pmatrix} (3 + 0.9\cos(\phi_2)_j)\cos(\phi_1)_i \\ -(3 + 0.9\cos(\phi_2)_j)\sin(\phi_1)_i \\ 0.9\sin(\phi_2)_j \end{pmatrix}, \tag{84}$$

where the initial normal vectors again come from cross-products of center differences.

In order to compare the performance of this algorithm to the technique of [28], we choose $N_1 = 41$ and $N_2 = 101$. We continue in steps of 0.1 from $\lambda = 1.0$ to $\lambda = 12.8$. Above that value, the Newton iterations fail to converge irrespective of the step size. We re-distribute by arc length along each meridian every 10 continuation steps. All parameters in the Newton iteration (e.g., convergence criterion, differencing technique) are the same in this example as for Example 6.1. Condition numbers range from about 800 to about 10^8, with a median of approximately 1800.

Fig. 5 shows the results of the method. The center line is not a periodic orbit in this example—it is just an average of the points in each meridian, placed on the plot to aid visualization. As before, the grid does not always lie directly in the plane $x_2 = 0$, so some of the curves are linear interpolations. The plot contains curves for λ from 1.0 to 12.0 in increments of 1.0 as well as additional λ values at 12.5 and 12.8. Clearly, the technique is not particularly penalized by a lack of quasi-periodic motion.

Remark 6.1. Phase-locked regions do lead to closed, invariant sub-manifolds in the form of periodic orbits, and the current method is not guaranteed to be stable in such situations. Nevertheless, even in these situations the method

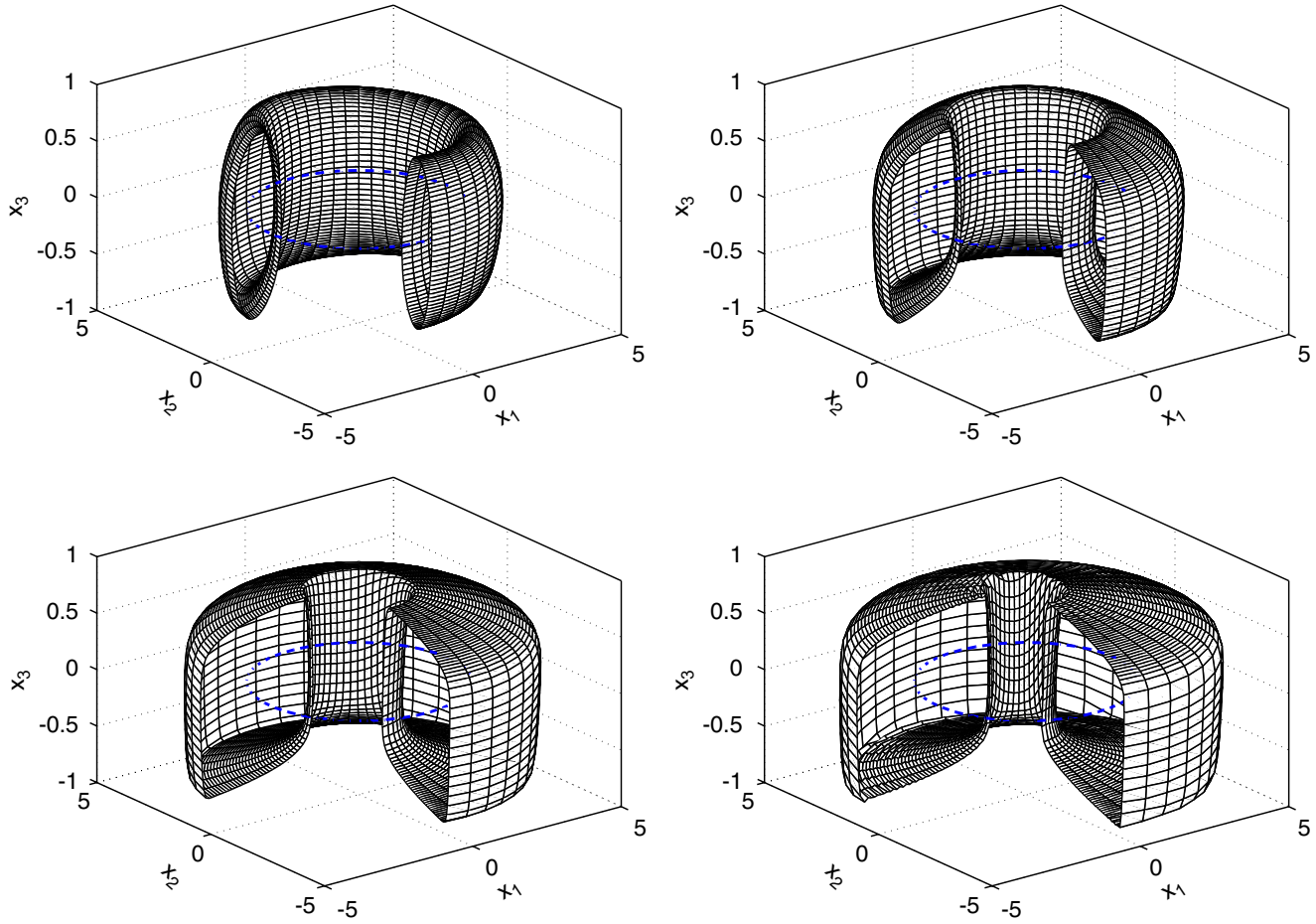

Fig. 5. Torus in forced circuit; $\lambda = 1.0,5.0,10.0$, and 12.8 (l to r, top to bottom).

appears to work properly, as long as the grid does not line up along one of the orbits. The next example illustrates this point.

6.3. Coupled oscillators

The next example is a 2-torus in $\mathbb{R}^4$, which tests the general algorithm with the full implementation to retrieve the normal vectors. We consider the following system of two linearly coupled planar oscillators:

$$\begin{aligned}
\dot{x}_1 &= \alpha x_2 + x_1(1 - x_1^2 - x_2^2) - \lambda(x_1 + x_2 - x_3 - x_4),\\
\dot{x}_2 &= -\alpha x_1 + x_2(1 - x_1^2 - x_2^2) - \lambda(x_1 + x_2 - x_3 - x_4),\\
\dot{x}_3 &= \alpha x_4 + x_3(1 - x_3^2 - x_4^2) + \lambda(x_1 + x_2 - x_3 - x_4),\\
\dot{x}_4 &= -\alpha x_3 + x_4(1 - x_3^2 - x_4^2) + \lambda(x_1 + x_2 - x_3 - x_4),
\end{aligned} \tag{85}$$

where we fix $\alpha = 0.55$ for comparison to previous studies [6,8,22,26].

At $\lambda = 0$, the system consists of two uncoupled, planar oscillators. Each oscillator has an attracting periodic orbit of unit radius and period $2\pi/\alpha$, and the cartesian products of these orbits trivially form an invariant 2-torus embedded in $\mathbb{R}^4$ for the whole system. As λ increases, the invariant torus persists, with two periodic orbits on its surface: one attracting, the other repelling. The attracting orbit lies on the intersection of the torus and the $(x_1 = x_3, x_2 = x_4)$ plane, and the repelling orbit lies on the intersection of the torus and the $(x_1 = -x_3, x_2 = -x_4)$ plane [1]. Equilibria develop on the second periodic orbit at $\lambda = \alpha/2$, but the torus actually breaks down before, when it loses its attractivity at $\lambda \approx 0.2605$ [20,26].

The initial $\overline{\mathbf{x}}$ at $\lambda = 0$ is a grid on the exact torus,

$$\overline{\mathbf{x}}((\phi_1)_i, (\phi_2)_j) = \overline{\mathbf{x}}_{i,j} = (\cos(\phi_1)_i \;\; \sin(\phi_1)_i \;\; \cos(\phi_2)_j \;\; \sin(\phi_2)_j)^{\mathrm{T}}, \tag{86}$$

and the initial normal vectors are

$$\overline{Q}_{i,j} = \begin{pmatrix} \cos(\phi_1)_i & \sin(\phi_1)_i & 0 & 0 \\ 0 & 0 & \cos(\phi_2)_j & \sin(\phi_2)_j \end{pmatrix}^{\mathrm{T}}, \tag{87}$$

where $(\phi_1)_i = 2\pi(i-1)/N_1$ and $(\phi_2)_j = 2\pi(j-1)/N_2$.

The Jacobian in this case is still periodic block bi-diagonal, but each sub-block is now periodic *block* bi-diagonal with full 2×2 blocks. The Jacobian is $2N_1N_2 \times 2N_1N_2$ with $16N_1N_2$ possible non-zero entries, and each high-level block contains $4N_2^2$ entries when full. For the values of N_1 and N_2 in the present study, this memory requirement is well within the reach of standard direct solution techniques and condition number estimators.

At first glance, it seems that the method might not work well for this torus because it has invariant sub-manifolds, namely the periodic orbits. As it turns out, however, difficulties only show up when the discretization lines up at positive λ values with at least one of the two planar periodic orbits.

The following observations from numerical experiments show how the method is sensitive to the choice of number of discretization points:

(i) If N_1 and N_2 are both even, then the Jacobian is numerically singular at $\lambda = 0$.
(ii) If $N_1 = N_2$ and odd, then the Jacobian is poorly conditioned as soon as $\lambda > 0$ (e.g., the condition number is of order 10^{11} for a 45×45 torus).
(iii) If $N_1 = N_2 \pm 1$, then the Jacobian is generally well-conditioned, and the method has no apparent problem continuing the torus.

The first observation is most likely related to the observed ill-conditioning in the method for an even–even 2-torus in $\mathbb{R}^3$. The second observation is probably related to the fact that if $N_1 = N_2$, then the grid lines up exactly along at least one of the two periodic orbits. One simple way to prevent this is to choose N_1 to be slightly different from N_2, which explains the third observation.

We are able to continue the branch of invariant tori up to $\lambda = 0.2605$, which is at, or near, breakdown. The continuation step size shrinks from $\Delta\lambda = 0.05$ near $\lambda = 0$ to $\Delta\lambda = 0.0005$ at the end. As with the 2-tori in $\mathbb{R}^3$, the largest expense is the generation of the Jacobian, and much of this is probably due to the use of `Matlab` instead of a lower-level language to perform all of the local (and hence looped) derivative approximations.

Because the torus distorts throughout the continuation process, the grid tends to skew. If left uncorrected, many of the boxes would become pinched, and the method would break down. It is therefore necessary to re-distribute points on the grid occasionally in a logical way.

There is no canonical mesh-distribution strategy for 2-tori. The method based on quasi-conformal mapping proposed by Moore [22] seems to work well, but requires considerable extra computation. For this particular example, practice has shown that a simple and effective correction strategy for a 45×46 torus is (1) re-distribute according to arc length along each longitude (sections of the form $\overline{\mathbf{x}}_{i,t}$, t constant), and then (2) independently re-distribute along each meridian (sections of the form $\overline{\mathbf{x}}_{t,i}$, where t is constant). This strategy is best applied after convergence, up through $\lambda = 0.25$, after which the torus does not undergo any further re-distribution.

Figs. 6 and 7 show the tori and the intersections of the tori with two planes. The solid line corresponds to the $x_{1,2} = x_{3,4}$ plane, so it indicates the stable periodic orbit. Similarly, the dashed line corresponds to the $x_{1,2} = -x_{3,4}$ plane, so it indicates the unstable periodic orbit.

Calculating the planar intersections is itself not a simple task. The lines on Figs. 6 and 7 represent averaged linear interpolants of where the grid lines of the torus cross the planes of interest. The intersection between the $x_{1,2} = -x_{3,4}$ plane and the torus seems to become non-transverse at breakdown, so the discrete grid only crosses that plane at a few scattered points. Fig. 7 therefore shows only discrete points for which the difference between components changes sign.

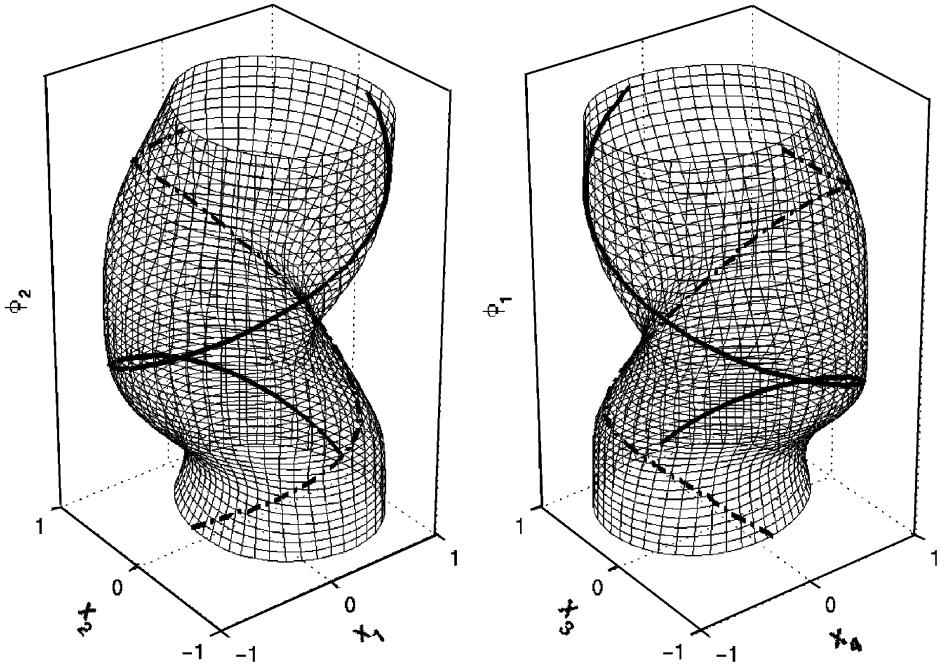

Fig. 6. Oscillators with planar intersections; $\lambda = 0.25$.

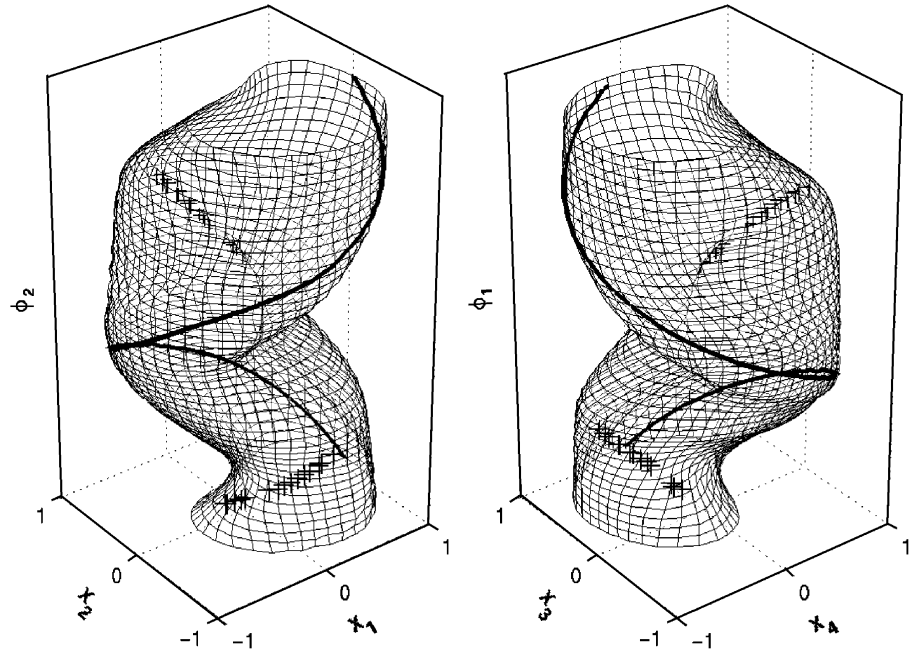

Fig. 7. Oscillators with planar intersections; $\lambda = 0.2605$.

7. Conclusions

In this paper we have studied a mid-point discretization scheme based on the "orthogonality condition" for the approximation of invariant tori, originally introduced in [22].

We made several contributions. We gave explicit details to show that formulating invariance through the orthogonality condition is equivalent at the smooth level to invariance formulated through the so-called PDE condition. We proved

that the method is unconditionally stable and consistent for periodic orbits in arbitrary-dimensional space. We proved that the method for 2-tori in $\mathbb{R}^3$ is unconditionally *unstable* when one uses an even number of discretization points in both angular directions. Numerical experiments showed that similar constraints apply more generally to p-tori in $\mathbb{R}^n$. Likewise, numerical experiments indicated that the presence of closed, invariant sub-manifolds can also cause instabilities. Adapting the algorithm to account for these difficulties, we presented numerical results showing that the end method is capable of approximating tori of practical interest at least as reliably as other competing methods, say those of [6,8,26,28].

Our main theoretical contribution is probably the negative result of stability of the basic scheme for 2-tori in $\mathbb{R}^3$. This negative result has led us to improved understanding of how to stabilize the method in practice. Regretfully, many existing works on approximation of invariant tori lack a rigorous stability analysis of the proposed numerical methods, and we suspect that a negative result similar to our own will apply to other techniques as well (see Remark 2.1).

To make progress toward understanding of techniques based on the orthogonality condition, we have made some simplifications with respect to the original work [22]. Most notably we have not analyzed or implemented the mesh-redistribution strategy proposed therein. It is possible that the mesh re-distribution technique has a stabilizing effect on the basic scheme we analyzed, in a similar way to the practical remedies we adopted in our numerical experiments, but rigorously inferring any of this will be very difficult.

References

[1] D.G. Aronson, E.J. Doedel, H.G. Othmer, An analytical and numerical study of the bifurcations in a system of linearly-coupled oscillators, Phys. D. 25 (1987) 20–104.

[2] U.M. Ascher, R.M. Mattheij, R.D. Russell, Numerical Solution of Boundary Value Problems for Ordinary Differential Equations, Prentice-Hall, Englewood Cliffs, NJ, 1988.

[3] H. Broer, H. Osinga, G. Vegter, Algorithms for computing normally hyperbolic invariant manifolds, Z. Angew. Math. Phys. 48 (1997) 480–524.

[4] X. Cabré, E. Fontich, R. de la Llave, The parametrization method for invariant manifolds i: manifolds associated to non-resonant subspaces, Indiana Univ. Math. J. 52 (2003) 283–328.

[5] X. Cabré, E. Fontich, R. de la Llave, The parametrization method for invariant manifolds ii: regularity with respect to parameters, Indiana Univ. Math. J. 52 (2003) 329–360.

[6] L. Dieci, G. Bader, Solution of the systems associated with invariant tori approximation II: multigrid methods, SIAM J. Sci. Comput. 15 (1994) 1375–1400.

[7] L. Dieci, J. Lorenz, Block M-matrices and computation of invariant tori, SIAM J. Sci. Statist. Comput. 13 (1992) 885–903.

[8] L. Dieci, J. Lorenz, Computation of invariant tori by the method of characteristics, SIAM J. Numer. Anal. (1995) 1436–1474.

[9] E.J. Doedel, R.C. Paffenroth, A.R. Champneys, T.F. Fairgrieve, Y.A. Kuznetsov, B.E. Oldeman, B. Sandstede, X.J. Wang, AUTO2000: software for continuation and bifurcation problems in ordinary differential equations, Technical Report, California Institute of Technology, Pasadena, CA 91125, 2000.

[10] L. Dieci, J. Lorenz, R.D. Russell, Numerical calculation of invariant tori, SIAM J. Sci. Statist. Comput. 12 (1991) 607–647.

[11] B. Krauskopf, H.M. Osinga, Investigating torus bifurcations in the forced van der Pol oscillator, IMA Vol. Math. Appl., vol. 119, Springer, New York, 2000, pp. 199–208.

[12] K. Edoh, R.D. Russell, W. Sun, Computation of invariant tori by orthogonal collocation, Appl. Numer. Math. 32 (2000) 273–289.

[13] T. Ge, Y.T. Leung, Construction of invariant torus using Toeplitz Jacobian matrices, fast Fourier transform approach, Nonlinear Dyn. 15 (1998) 283–305.

[14] G.H. Golub, C.F.V. Loan, Matrix Computations, third ed., Johns Hopkins University Press, Baltimore, 1996.

[15] J. Guckenheimer, P. Holmes, Nonlinear Oscillations, Dynamical Systems, and Bifurcations of Vector Fields, Applied Mathematical Sciences, vol. 42, Springer, New York, 1985.

[16] J. Hale, Ordinary Differential Equations, second ed., Krieger, Malabar, Florida, 1980.

[17] À. Jorba, Numerical computation of the normal behaviour of invariant curves of n-dimensional maps, Nonlinearity 14 (2001) 943–976.

[18] À. Jorba, J. Villanueva, On the persistence of lower-dimensional invariant tori under quasi-periodic perturbations, J. Nonlinear Sci. 7 (1997) 427–473.

[19] H.B. Keller, Numerical Methods in Bifurcation Problems, Springer, Berlin, 1987.

[20] L. Dieci, J. Lorenz, Lyapunov-type numbers and torus breakdown: numerical aspects and a case study, SIAM J. Sci. Statist. Comput. 14 (1997) 79–103.

[21] R. de la Llave, C.E. Wayne, Whiskered and low dimensional tori in nearly integrable Hamiltonian systems, Math. Phys. Electron. J. 10 (2004) Paper 5, 45pp. (electronic).

[22] G. Moore, Computation and parameterization of invariant curves and tori, SIAM J. Numer. Anal. 15 (1991) 245–263.

[23] G. Moore, Geometric methods for computing invariant manifolds, Appl. Numer. Math. 12 (1991) 607–647.

[24] H. Osinga, Computing invariant manifolds, Ph.D. Thesis, Rijksuniversiteit Groningen, The Netherlands, 1996.

[25] B. Rasmussen, Numerical methods for the continuation of invariant tori, Ph.D. Thesis, Georgia Institute of Technology, Atlanta, 2003.

[26] V. Reichelt, Computing Invariant Tori and Circles in Dynamical Systems, IMA Vol. Math. Appl., vol. 119, Springer, New York, 2000, pp. 407–437.
[27] W. Rheinboldt, On the computation of multi-dimensional solution manifolds of parametrized equations, Numer. Math. 53 (1988) 165–181.
[28] F. Schilder, H. Osinga, W. Vogt, Continuation of quasi-periodic invariant tori, SIAM J. Appl. Dyn. Syst. 4 (3) (2005) 459–488.
[29] M.R. Trummer, Spectral methods in computing invariant tori, Appl. Numer. Math. 34 (2000) 275–292.
[30] M.V. Veldhuizen, A new algorithm for the numerical approximation of an invariant curve, SIAM J. Sci. Statist. Comput. 8 (1987) 951–962.